

1 **The changing character of ~~twenty-first~~21st century precipitation over the**

2 **western United States in the variable-resolution CESM**

3 Xingying Huang, * Paul A. Ullrich

4 *Department of Land, Air and Water Resources, University of California, Davis*

5 *Corresponding author address: Xingying Huang, Department of Land, Air and Water Resources,
6 University of California Davis, Davis, CA 95616.
7 E-mail: xyhuang@ucdavis.edu

ABSTRACT

8 The changing characters of precipitation frequency and intensity have been
9 comprehensively investigated from recent historical period to the end of the
10 21st century over the western United States. Variable-resolution Community
11 Earth System Model (VR-CESM) ensemble simulations are applied with a
12 fine grid resolution of $\sim 0.25^\circ$ over the study area. Simulations are forced
13 with prescribed sea-surface temperatures, sea-ice extent and greenhouse gas
14 concentrations from the representative concentration pathway (RCP) 8.5 sce-
15 nario. VR-CESM is shown to be effective at accurately capturing the spatial
16 patterns of the historical precipitation climatology. The results of VR-CESM
17 output provide significantly regional details with crucial enhancement of pre-
18 cipitation representations over complex terrain. In the Intermountain West
19 and Southwest U.S., we observe a statistically significant increase in mean
20 precipitation and rainy days through mid-century, although this trend is tam-
21 pered by end of century in response to a decrease in relative humidity. Over
22 the Pacific Northwest, extreme precipitation events are observed to increase
23 significantly as a result of increased cool season integrated vapor transport as-
24 sociated with a moistening of the cool seasons and drying through the warm
25 seasons. In particular, extreme precipitation in this region appears to increase
26 more rapidly than would be predicted by the Clausius-Clapeyron relationship.
27 No clear climate signal emerges in mean precipitation or extreme events in the
28 majority of California, where the precipitation climatology is attributed with
29 large interannual variabilities that are tied closely to ENSO patterns.

30 **1. Introduction**

31 There is substantial and growing interest in understanding the character of precipitation within
32 a changing climate, motivated largely by its pronounced impacts on water availability and flood
33 management in both human and natural systems (Hegerl et al. 2004; Kharin et al. 2007; Scoc-
34 cimarro et al. 2013). Among past studies addressing precipitation, extremes have been a major
35 focus, particularly drought and flood events (Seneviratne et al. 2012). Overall, it is widely agreed
36 that although atmospheric water vapor concentration is increasing, the impacts of a changing cli-
37 mate on the character of precipitation is far more complicated. Extreme precipitation events are
38 particularly nuanced: Our best projections suggest that extreme precipitation events will intensify
39 even in regions where mean precipitation decreases (Tebaldi et al. 2006; Kharin et al. 2007).

40 ~~Future climate~~ Climate projections, particularly those addressing the frequency and inten-
41 sity of rare events, are inevitably subject to large uncertainties. Nonetheless, climate models
42 have been invaluable tools for developing insight into this problem (Easterling et al. 2000). In
43 particular, global climate models (GCMs) have often been used to investigate changes in the
44 mean, variability and extremes of climate, as forced with predicted greenhouse gas (GHGs)
45 concentrations and aerosol emissions (Meehl et al. 2006). ~~Although several past~~ For examples,
46 Kharin et al. (2013) found amplified changes (2-3 times) in extreme precipitation compared to
47 mean precipitation in the CMIP5 (the Coupled Model Intercomparison Project Phase 5) models
48 globally-averaged. Generally, models agree better on the response of extreme precipitation in
49 the extratropics with relatively well represented precipitation-driven dynamics in GCMs than the
50 tropics and subtropics (Kharin et al. 2013; Pendergrass et al. 2015) .

51 Although quite a few studies have investigated climate extremes at the global scale (Senevi-
52 ratne et al. 2012), studies addressing extremes at local and regional scales are less common.

53 It is well understood how increased GHG concentrations have contributed to the observed in-
54 tensification of heavy precipitation events over the tropical ocean (Allan and Soden 2008) and
55 the majority of Northern Hemisphere overland areas (Min et al. 2011), but changes are much
56 more poorly understood at regional scales where meteorological variability is large (Trenberth
57 2011). ~~As a consequence of this variability, confidence in the assessment of regional extreme~~
58 ~~precipitation changes requires both high spatial resolution and a long integration period, both of~~
59 ~~which can make the computational cost untenable for global simulations~~ Moreover, GCMs tend
60 ~~to underestimate observed precipitation magnitudes both in the aspects of mean precipitation and~~
61 ~~precipitation extremes, implying the necessity of downscaling techniques (Sillmann et al. 2013a)~~.
62 This issue of insufficient regional-scale climate information has been a major outstanding problem
63 in climate science, as stakeholders and water managers typically require fine-scale information on
64 climate impacts in order to effectively develop adaptation and mitigation strategies.

65 As a consequence, confidence in the assessment of regional extreme precipitation changes
66 requires both high spatial resolution and a long integration period, both of which can make the
67 computational cost untenable for global simulations. Dynamical downscaling with regional cli-
68 mate models (RCMs) has been one of the few tools available to ~~asecertain achieve~~ the frequency, in-
69 tensity, and duration of extreme events at the needed scales. By only simulating a limited regional
70 domain, RCMs better capture fine-scale dynamical features with high horizontal resolution (Bell
71 et al. 2004; Frei et al. 2006; Rauscher et al. 2010; Wehner 2013). Higher resolution enables more
72 accurate simulation of precipitation extremes, ~~which are driven by~~ with better-resolved circulation
73 patterns, ~~cloudiness~~ cloud distributions, land use, ~~land/water contrast, snowpack and topography~~
74 features, snowpack and orographic effects (Leung et al. 2003a; Diffenbaugh et al. 2005; Salathé Jr
75 et al. 2008; Wehner et al. 2010). For example, Leung et al. (2003b) showed that the higher-
76 resolution RCMs yield more realistic precipitation patterns and produce more frequent heavy pre-

77 cipitation over the western U.S. (WUS), consistent with observations. Diffenbaugh et al. (2005)
78 studied both extreme temperature and precipitation events over the contiguous United States using
79 ~~a-an~~ RCM configured at 25 km horizontal resolution, and demonstrated that fine-scale processes
80 were critical for accurate assessment of local- and regional-scale climate change vulnerability.
81 ~~Salathé Jr et al. (2008) found significant differences in trends for temperature and precipitation~~
82 ~~over the Pacific Northwest using a high-resolution RCM for future climate simulations. And~~
83 ~~Ashfaq et al. (2016) observed~~ In the study of Ashfaq et al. (2016), a 7.4% increase in precipita-
84 tion from extremes ~~is projected with every 1°C rise in surface temperature~~ over the contiguous
85 U.S. ~~from simulations with using~~ RegCM4 ~~simulations~~ driven by CMIP5 ~~global data~~ data, when
86 ~~comparing historical period (1965-2005) to near-term future period (20102050).~~

87 ~~Despite their success~~ However, RCMs also have known issues associated with inconsistency
88 between the lateral forcing data and the driven RCM. The menu of physical parameterizations
89 and tuning parameters typically available to RCMs can also lead to over-tuning of the model
90 for a particular geographic region or climatological field (McDonald 2003; Laprise et al. 2008;
91 Mesinger and Veljovic 2013). Consequently, there has been growing interest in utilizing variable-
92 resolution enabled GCMs (VRGCMs) to improve implement regional climate simulations. Unlike
93 RCMs, which require GCM data to drive the simulation at lateral boundaries, VRGCMs use a
94 unified model with ~~eoarse global resolution and~~ enhanced resolution over a specific study region
95 ~~while keeping the coarse resolution at remaining global area~~ (Staniforth and Mitchell 1978; Fox-
96 Rabinovitz et al. 1997). VRGCMs have demonstrated a competitive ability for regional climate
97 studies at a reduced computational cost, particular when compared to uniform-resolution GCMs
98 (Fox-Rabinovitz et al. 2006; Rauscher et al. 2013).

99 In this paper, we utilize the recently developed variable-resolution option in the Community
100 Earth System Model (VR-CESM). VR-CESM is based on the CESM (and its predecessor,

the Community Climate System Model (CCSM)), a family of models that have been used for decades to study the global climate (Neale et al. 2010a; Hurrell et al. 2013). The overall performance of VR-CESM for modeling regional climate in the California and Nevada is detailed in Huang et al. (2016), where it was argued that VR-CESM has competitive biases in comparison to the Weather Research and Forecasting (WRF) model (a traditional RCM) and the uniform-resolution CESM, when evaluating against high-quality observations and reanalysis. VR-CESM has already been used in a number of studies to simulate fine-scale atmospheric processes (Zarzycki et al. 2014, 2015; ?; Huang and Ullrich 2016; ?) (Zarzycki et al. 2014, 2015; Rhoades et al. 2016)

This study focuses on changes in the character of precipitation over the 21st century within the WUS, as predicted from long-term ensemble runs conducted with VR-CESM with a local grid resolution of $\sim 0.25^\circ$. The WUS is known to be particularly vulnerable to hydrological extremes, particularly floods and droughts (Leung et al. 2003b; Caldwell 2010), and hosts a variety of local features and microclimates associated with its rough and varied topography. Simulations of the future climate are performed in accordance with the representative concentration pathway (RCP) 8.5 scenario, which describes a “business-as-usual” projection for GHGs (Riahi et al. 2011). In this study, we focus singularly on the RCP 8.5 scenario because its mid-century results are similar to a more optimistic RCP2.6 scenario end-of-century. ~~Simulations are further conducted Global sea surface temperatures (SSTs) and sea ice, which are used to compute ocean-atmosphere fluxes, are prescribed in accordance with the widely-used Atmospheric Model Intercomparison Project (AMIP) protocol (Gates 1992), a widely-used approach for climate model diagnosis, validation and intercomparison that imposes global sea surface temperatures (SSTs) and sea ice. It is well-known that correctly simulating changes to the spatial pattern of SSTs in state-of-the-art coupled GCMs remains a significant challenge (Joseph and Nigam 2006; Stevenson 2012; Jha et al. 2014; Taschetto et al. 2014).~~

¹²⁵ ~~However, by~~ By constraining atmospheric boundary conditions at the sea surface, we
¹²⁶ avoid model biases that are known to exist significantly in the fully coupled configura-
¹²⁷ tion (~~Grodsky et al. 2012; Small et al. 2014~~) to simulate changes to the spatial pattern of SSTs
¹²⁸ (~~Joseph and Nigam 2006; Grodsky et al. 2012; Stevenson 2012; Jha et al. 2014; Small et al. 2014~~).■
¹²⁹ but accept potential uncertainties associated with our choice of SSTs.

¹³⁰ Changes in the character of precipitation, in terms of frequency and intensity at multiple levels,
¹³¹ have been assessed in our study from recent history through the end of the 21st century. A com-
¹³² prehensive set of indices for precipitation extremes ~~have has~~ been evaluated from the ensemble
¹³³ simulations over ~~the each~~ 26-year ~~periods~~ period corresponding to historical (1980-2005), mid-
¹³⁴ century (2025-2050) and end-of-century (2075-2100). Spatial inhomogeneity in local geography
¹³⁵ and temperature are observed to result in similarly inhomogeneous impacts on the precipitation
¹³⁶ field. Teleconnections (specifically the El Niño-Southern Oscillation, ENSO) are also observed to
¹³⁷ have a pronounced impact on precipitation features. Since only one SST dataset was used for this
¹³⁸ study, we note that our projections are conditioned on a particular future character of ENSO. This
¹³⁹ is a potentially large source of uncertainty, as at present there is no clear consensus on how ENSO
¹⁴⁰ may behave under a warming climate (Fedorov and Philander 2000; Latif and Keenlyside 2009;
¹⁴¹ Guilyardi et al. 2009; Collins et al. 2010; DiNezio et al. 2012), and strengthening or weakening of
¹⁴² this pattern will have clear consequences for our results (as discussed in section 6d).

¹⁴³ This work builds on a number of previous studies that have explored the projected future change
¹⁴⁴ in WUS precipitation. For example, Kim (2005) applied downscaled climate change signals to se-
¹⁴⁵ lected indicators, and concluded that global warming induced by increased CO₂ is likely to drive
¹⁴⁶ increases in extreme hydrologic events in the WUS. Duffy et al. (2006) found that changes to
¹⁴⁷ mean precipitation predicted by the RCMs are not statistically significant compared to interannual
¹⁴⁸ variability in many regions over WUS, although there is little consistency among the different

149 RCMs as to responses in precipitation to increased GHGs. Gao et al. (2015) pointed out a poten-
150 tially large increase in atmospheric river events by the end of the 21st century under the RCP8.5
151 scenario, with implications for large-scale and heavy precipitation events along the Pacific coast.

152 This paper is structured as follows. Section 2 describes the model setup ~~-and~~ Section 3 describes
153 the methodology and reference datasets employed. An assessment of the ability of the model to
154 capture the historical climatology of the WUS is given in section 4 with discussions of drivers of
155 precipitation change in section 5. Results from the future mean climatological trend and projected
156 changes to precipitation indices are in section 6. Section 7 summarizes the main points of the
157 study along with a further discussion.

158 2. Model Setup

159 CESM is a state-of-the-art Earth modeling framework, consisting of coupled atmosphere,
160 ocean, land and sea ice models (Neale et al. 2010b; Hurrell et al. 2013). In this study, the
161 Community Atmosphere Model version 5 (CAM5) (Neale et al. 2010b) and the Community
162 Land Model version 4.0 (Oleson et al. 2010) are used. CAM5 is configured with the Spectral
163 Element (SE) dynamical core, which is known for its conservation properties, accuracy and
164 parallel scalability (Dennis et al. 2011; Taylor 2011) and incorporates the variable-resolution
165 option (Zarzycki et al. 2014). CLM is employed in the *unigrid* configuration, which al-
166 lows the land model and atmospheric model to utilize the same model grid so eliminates
167 the need for interpolation. ~~SSTs and sea ice, which are used to compute ocean-atmosphere~~
168 ~~fluxes, are prescribed in accordance with the AMIP protocol (Gates 1992)~~. The variable-
169 resolution mesh used for this study is depicted in Figure 1, in accord with our past studies
170 (~~?Huang et al. 2016; Huang and Ullrich 2016; ?~~) (Rhoades et al. 2016; Huang et al. 2016; Huang and Ullrich

171 Simulations have been performed for the historical period (1979-2005, hereafter referred to as
172 hist) and for two future periods: 2024-2050 (hereafter referred to as mid) and 2074-2100 (hereafter
173 referred to as end). Daily ~~output~~ outputs are recorded for each period on the native SE grid
174 and then remapped to a regional latitude-longitude mesh (Ullrich and Taylor 2015; Ullrich et al.
175 2016). ~~For purposes of analysis, the~~ The first year of each time period was discarded as a spin-up
176 period to allow adequate time for the initialized land and atmosphere to equilibrate. The 26-year
177 duration was chosen to provide an adequate sampling of annual variability for each time phase.
178 As mentioned earlier, GHG concentrations are set based on RCP8.5. Historical SSTs and sea ice
179 are prescribed at 1° resolution, as described by Hurrell et al. (2008). SSTs and sea ice for each
180 future period are developed from fully-coupled RCP 8.5 climate simulations from CESM with
181 bias correction applied (Cecile Hannay, personal communication). Annually-updated land surface
182 datasets, which prescribe land-use characteristics, are interpolated from 0.5° to the land model
183 grid.

184 Ensemble runs are needed to ensure that the sample adequately accounts for climate variability,
185 especially for statistics associated with climatological extremes. However, the exact number of
186 ~~ensemble members required~~ required ensemble members is heavily dependent on the variability
187 of the particular metric being examined, and so no standard ensemble criteria ~~exists~~ exist. Deser
188 et al. (2012b) suggest that around 3 ensemble runs are required to detect a significant epoch dif-
189 ference for JJA (June-July-August) surface temperatures, whereas 10 to 30 ensemble members are
190 needed for that for DJF (Dec.-Jan.-Feb.) precipitation. In our study, the use of prescribed SSTs
191 does reduce the intrinsic variability of the climate system (~~see supplement Figure S1~~), largely
192 and so we found reasonably converged results with two ensemble members for the historical pe-
193 riod and four ensemble members for each future period ~~—(see supplement Figure S1-S3 for the~~
194 inter-member variability). Although means from multiple models are better for simulating the

195 climate variability, the accuracy might be reduced due to compensation of the results from both
196 good models and fair models. Using a high-quality model with reduced signal noise, our aim in this
197 study is to understand how precipitation is supposed to be changed in diverse climate regions in the
198 future, and what are the main mechanisms that drive corresponding changes with better-resolved
199 fine-scale dynamical processes. Even using different models, we suppose the physical relationship
200 and spatial characteristics still hold.

201 3. Methodology

202 a. Precipitation indices

203 Standard indices have been employed to characterize precipitation
204 (Tebaldi et al. 2006; Zhang et al. 2011; Sillmann et al. 2013b). In order to choose a
205 comprehensive (but minimal) set that ~~are~~is informative to stakeholders and water
206 ~~resource~~ managers, indices from throughout the literature were compiled ~~to~~ characterize
207 precipitation (Tebaldi et al. 2006; Zhang et al. 2011; Sillmann et al. 2013b). The in-
208 dices examined include those defined by the Expert Team on Climate Change De-
209 tection and Indices (ETCCDI) (Karl et al. 1999) that are featured in earlier studies
210 (Dulière et al. 2011; Sillmann et al. 2013b; Diffenbaugh et al. 2005; Singh et al. 2013) (Diffenbaugh et al.
211 others such as return levels, dry spell and wet spell characteristics defined by either percentiles or
212 by selected thresholds. ~~As a result,~~

213 From our standpoint, interpreting precipitation events with different intensities is more
214 straightforward, relevant for societal impacts (Alexander et al. 2006), and informative to water
215 resources management and climate adaptation strategies. Therefore, the indices we have chosen
216 for this study attempt to provide a relatively comprehensive characterization of precipitation, and

²¹⁷ are summarized in Table 1. Indices related to dry spells of variable duration have been investigated
²¹⁸ in this study, but only exhibited significant differences for extremely short ($\text{< } 5 \text{ day} \leq 5 \text{ days}$) dry
²¹⁹ spells and so are not included in our results.

²²⁰ *b. Impacts of ENSO*

²²¹ The impact of ENSO ~~on precipitation~~ is emphasized in our study due to its significant influence
²²² on precipitation over a majority of our study area, particularly the southwest U.S. (Cayan et al.
²²³ 1999; Zhang et al. 2010; Deser et al. 2012a; Yoon et al. 2015). The phase of ENSO (*i.e.* El Niño
²²⁴ and La Niña) is identified each year using the Oceanic Niño Index (ONI), defined as the 3-month
²²⁵ running means of SST anomalies in the Niño 3.4 region (covering 5N-5S, 120-170W based on
²²⁶ NOAA (2013)). An El Niño or La Niña episode is said to occur when the ONI exceeds +0.5 or
²²⁷ -0.5 for at least five consecutive months for a water year (*i.e.* from July to June) (NOAA 2013) (see
²²⁸ the supplement Figure S2-S4 for the ONI values). In order to adjust for the trend in the SST field
²²⁹ associated with climate change, the anomaly is computed against the detrended mean SSTs from
²³⁰ the periods ~~1971-2000~~, 2020-2050 and 2070-2100 for ~~hist~~, mid and end respectively, using the
²³¹ aforementioned ~~observed and predicted SST datasets~~predicted SST dataset. As argued by Kao and
²³² Yu (2009), it may be desirable to use an extended Niño 3.4 region to determine the phase of ENSO
²³³ – however, when employing SST anomalies integrated over ~~the~~an extended region 105-170W, we
²³⁴ observed no significant impact on ONI statistics.

²³⁵ *c. Assessing statistical significance*

²³⁶ Student's t-test has been used to determine whether or not two datasets at each grid point are
²³⁷ statistically equivalent ~~, if when~~ the sample population can be adequately described by a normal
²³⁸ distribution. The normality of a dataset is assessed under the Anderson-Darling test. When the

239 sample populations do not approximately follow a normal distribution, Mann-Whitney-Wilcoxon
240 (MWW) test is employed in lieu of the t-test. All tests are evaluated at the 0.05 (α) significance
241 level. When comparing different time periods, statistical tests are conducted by treating all years
242 from all ensemble members as independent samples (26×2 sample years for hist and 26×4 sam-
243 ple years for mid and end). [Spatial correlation is assessed by computing Pearson product-moment](#)
244 [coefficient of linear correlation between climatological means from models and reference datasets.](#)

245

246 *d. Reference datasets*

247 Gridded observational datasets and reanalysis of the highest available quality, with comparable
248 horizontal resolutions to our VR-CESM simulations, are used for assessing the simulation quality.
249 [For comparison purpose, the reference dataset is interpolated to the model's grid resolution as](#)
250 [needed using bilinear interpolation methods.](#) Multiple reference datasets are necessary due to the
251 underlying uncertainty in the precipitation field. The three datasets employed are as follows:

252 **UW Gridded Data:** The 0.125° UW daily gridded meteorological data is obtained from
253 the Surface Water Modeling group at the University of Washington, covering the period
254 1949-2010 (Maurer et al. 2002; Hamlet and Lettenmaier 2005). The UW dataset imposes
255 topographic corrections by forcing the long-term average precipitation to match that of the
256 Parameter-elevation Regressions on Independent Slopes Model (PRISM) dataset.

257 **National Centers for Environmental Prediction (NCEP) Climate Prediction Center**
258 **(CPC):** The 0.25° CPC daily dataset provides gauge-based analysis of daily precipitation cov-
259 ering the period 1948-2006. It is a unified precipitation product that covers the Conterminous

United States and amalgamates a number of data sources at CPC via optimal interpolation
objective analysis.

North American Regional Reanalysis (NARR): The ~32 km NCEP NARR reanalysis provides 3-hourly precipitation snapshots, obtained by dynamical downscaling over North America and covering the period 1979-present (Mesinger et al. 2006).

4. Assessment of Precipitation Character in VR-CESM

Before proceeding, we assess the ability of VR-CESM to represent the character of precipitation over the WUS. The indices defined in Table 1 are depicted in Figures 2, 3 and 4 for VR-CESM and each of the reference datasets over the historical period (1980-2005). We assume equal confidence in each of the reference datasets, and use Student's t-test (with UW, CPC, and NARR as the three statistical samples) to identify regions where VR-CESM deviates significantly from the reference mean. Regions where differences are statistically significant in the VR-CESM dataset are identified with stippling. We acknowledge that NARR is certainly not as good at representing precipitation climatology as the gridded observations of CPC or UW (Huang et al. 2016). However, our purpose is to combine the gridded observations and high-quality reanalysis dataset together to understand the performance of VR-CESM in precipitation representation accounting for the uncertainty in those frequently used datasets.

Overall, VR-CESM accurately captures the spatial patterns of precipitation (with spatial correlation coefficients larger than 0.9 as compared to the observations) and its indices. As expected, the majority of precipitation is distributed along the northwest coast and the mountainous regions of the Cascades and the Sierra Nevada. Nonetheless, several apparent Specially, regional biases are present -with detailed descriptions as follows.

282 First, VR-CESM significantly overestimates Pr over dry regions with differences between 0.2
283 mm to 1.5 mm, and over the eastern flank of the Cascades and on both sides of the Sierra Nevada
284 (with relative differences reaching 50%-150%). As with many regional models, VR-CESM is
285 “dreary” and exhibits too many precipitation days ($R1mm$, $Pr \geq 1$ mm/day and $R5mm$, 1 mm/day \leq
286 $Pr \leq 5$ mm/day) (see Figure 2 and 3) (Stephens et al. 2010). The spatial correlations are about 0.85,
287 0.75, 0.8 and 0.9 for R1mm, R5mm, R10mm and R20mm compared to the references. Nonethe-
288 less, over most regions, the relative contribution of each precipitation frequency subset to total
289 precipitation (including F1mm, F5mm, F10mm, F20mm and F40mm) ~~agrees well, suggesting~~
290 ~~that the frequency distribution describing precipitation intensity is accurately simulated almost~~
291 ~~everywhere~~ is moderately represented by the model (with spatial correlations ranging from 0.7 to
292 0.8), suggesting a proper representation of the overall frequency distribution of the precipitation
293 intensity.

294 Second, the spatial pattern of precipitation intensity (SDII) ~~agrees~~ matches well between VR-
295 CESM and references ~~with agreement~~ (with spatial correlations around 0.85) everywhere except
296 in the Great Plains (the eastern edge of our domain) and in California’s Central Valley. The Great
297 Plains is not a focus of this study, ~~but and~~ the suppressed intensity is primarily during the warm
298 season (April-September) ~~and so~~, which likely represents a failure of the convection scheme to
299 adequately simulate variability in this region. This bias is also observed in CESM at 1° and 0.25°
300 uniform-resolution CESM simulations (Small et al. 2014), and so is not a symptom of the ~~eastern~~
301 ~~edge of the~~ variable-resolution transition region over the eastern edge.

302 However, the grossly exaggerated intensity over the western flank of the Sierra Nevada through
303 California’s Central Valley does merit some additional discussion. Here, the overestimation of pre-
304 cipitation and enhanced intensity is associated with too many extreme precipitation events ($Pr > 20$
305 mm/day) (see Figure 4, ~~F40mm and Fxmm for R40mm and Rxmm~~). This bias is related to ex-

306 aggerated orographic uplift (upslope winds) ~~and which also~~ triggers a dry bias along the eastern
307 flank of the Sierras. Similar biases in simulating extreme precipitation over topographically com-
308 plex regions have also been found in high-resolution RCM ~~smulationssimulations~~, and have been
309 primarily attributed to excessively strong winds (Walker and Diffenbaugh 2009; Singh et al. 2013).
310 This ~~bias is not alleviated by simply increasing the spatial resolution, as experimental VR-CESM~~
311 ~~simulations at 14km, 7km and 3.5km show only modest improvement (Alan M. Rhoades, personal~~
312 ~~communication). For VR-CESM, this~~ issue may be further impacted by the diagnostic treatment
313 of precipitation in CAM5 (Morrison and Gettelman 2008; Gettelman et al. 2008). ~~Recent work by~~
314 ~~Rhoades (personal communication) has shown that using prognostic MG2 microphysics routines~~
315 ~~can dramatically improve mountain precipitation climatology, as tested with an early version of~~
316 ~~CAM6. The bias might also be related to more complex dynamic processes or the lack of the~~
317 ~~scale-aware model parameterization schemes when producing the orographic forced precipitation.~~

318

319 The representation of precipitation in VR-CESM over California was also discussed in Huang
320 et al. (2016), where it was observed that VR-CESM simulations at 0.25° adequately represented re-
321 gional climatological patterns with high spatial correlation. VR-CESM demonstrated comparable
322 performance to WRF ~~at with a similar grid resolution of~~ 27 km (which was forced ~~with by~~ ERA-
323 Interim reanalysis) ~~, but still overestimated overall winter precipitation compared to reference~~
324 ~~datasets (by about 25%-35%), with the largest differences over the western edge of the Sierra~~
325 ~~Nevada. This bias is not alleviated by simply increasing the spatial resolution, as experimental~~
326 ~~VR-CESM simulations at 14km, 7km and 3.5km show only modest improvement (Alan M.~~
327 ~~Rhoades, personal communication). This suggests that the bias might be related with more~~
328 ~~complex dynamic processes rather than treatment of the orographic effects. showing significant~~
329 ~~improvement contrasted to CESM at $\sim 1^\circ$.~~

330 CESM at In order to better understand the impacts of resolution, CESM at $\sim 1^\circ$ resolution was
331 also assessed in order to better understand the impacts of resolution given as a contrast in the
332 supplement (see Figure S5). Overall, we find that precipitation patterns over complex topog-
333 raphy are poorly represented in the 1° dataset and do not capture without capturing the spatial
334 patterns induced by orographic effects. Over the Cascades and the Sierra Nevada, total precipi-
335 tation is grossly underestimated by the 1° data, even when compared to coarsened VR-CESM,
336 compared to gridded and reanalysis datasets(see the supplement Figure S3). Precipitation has oth-
337 erwise been smoothed out over the coastal areas and the mountainous regions of the northwest U.S
338 when simulated with CESM at coarse resolution. This result clearly underscores the benefits of
339 high resolution (particularly the representation of topography) in simulating precipitation features.
340 Results are also provided in the supplement The ability for GCMs to simulate extreme precipitation
341 also strongly depends on the horizontal resolution as discussed in Wehner et al. (2010) since
342 precipitation typically intensifies at high resolution (Rauscher et al. 2016; O'Brien et al. 2016).
343 A rough comparison is also provided (also see the supplement Figure S5) for the output from
344 a globally-uniform CESM run at 0.25° spatial resolution with the finite volume (FV) dynamical
345 core (Wehner et al. 2014), which exhibits exhibiting similar performance to VR-CESM(also see
346 the supplement Figure S3). Overall, VR-CESM at 0.25° resolution appears to provide the best
347 tradeoff between accuracy and computational cost, as the coarser resolution does not correctly
348 represent precipitation features and higher resolution does not appear to substantially improve
349 model accuracy (at least in this version of CAM).

350 We have also assessed the impact of the ENSO signal within the historical VR-CESM runs
351 by differencing the precipitation fields between the warm phase (i.e. El Niño) and cool phase
352 (i.e. La Niña), compared to references (see the supplement Figure S4). It is noticed that
353 ENSO exhibits a weaker signal for observational precipitation, compared to VR-CESM, which

354 might suggest that the model exaggerates ENSO's impact on precipitation, especially over the
355 northwest U.S. ~~The~~Therefore, the improvement of ENSO in the model is directly proportional to
356 the representation of ENSO-forced precipitation anomalies (AchutaRao and Sperber 2006).

357 **5. Drivers of Climatological Precipitation Change**

358 The remainder of this paper now focuses on model predictions of precipitation change over the
359 21st century. Precipitation has been observed and modeled to be ~~modified in character~~changed
360 at both global and regional scales under climate change. The observed intensification of heavy
361 precipitation events over the ~~the~~ recent past for the majority of Northern Hemisphere land areas
362 is primarily attributed to increases in GHGs (Min et al. 2011). GHGs drive radiative changes in
363 the lower troposphere, increase SSTs and lead to increased evaporation, all of which then impact
364 the character of precipitation events (Allen and Ingram 2002; Sugi and Yoshimura 2004). Several
365 studies have argued that precipitation extremes will intensify continuously through the end of ~~the~~
366 21st century in both dry and wet regions, although the extent of this change will be spatially
367 heterogeneous (Donat et al. 2016).

368 In accordance with the Clausius-Clapeyron (C-C) relationship, saturation vapor pressure in
369 the atmosphere is expected to increase by $\sim 7\%$ for each 1°C increase in temperature (Al-
370 lan and Soden 2008). As long as a source of water vapor is present, a corresponding
371 increase in atmospheric water vapor content is expected. Naturally, evaporation over the
372 ocean will ~~increase~~intensify with climate warming, but increases in water vapor content
373 over land may be constrained by soil moisture (Cayan et al. 2010). When specific humid-
374 ity is high, heavy rain events become more probable, even if total precipitation is decreasing
375 (~~Trenberth 2011~~)(Allen and Ingram 2002; Trenberth 2011). This suggests that global total pre-
376 cipitation is expected to increase at a slower rate than precipitation extremes (Allan and Soden

377 2008). In accordance with previous studies (e.g. Allan and Soden (2008); O’Gorman and Schnei-
378 der (2009); Min et al. (2011)), changes to extreme precipitation follow the C-C relationship more
379 closely than total precipitation amount (Trenberth et al. 2003). However, there is still substan-
380 tial uncertainty regarding the magnitude of this change, since precipitation extremes are also de-
381 pendent on factors such as the vertical velocity profile and ~~temperature~~thermodynamic effects
382 (O’Gorman and Schneider 2009).

383 With overland water vapor constrained by soil moisture content, changes to moderate or heavy
384 precipitation events (occurred mainly in cool seasons) over the WUS are mainly the result of in-
385 creased large-scale vapor transport from the eastern Pacific Ocean rather than directly from evap-
386 oration, typically associated with atmospheric rivers (ARs) and/or orographic uplift (Trenberth
387 et al. 2003; Neiman et al. 2008). Warming may lead to enhancement of the storm track, which
388 would increase ARs along the U.S. west coast with increased air water vapor content in the future
389 (Dettinger 2011; Gao et al. 2015).

390 The ~~In addition, the~~ precipitation of the WUS has strong inter-annual variability caused by large-
391 scale atmospheric circulation mainly associated with the ENSO (Leung et al. 2003b). As a signif-
392 icant driver of precipitation, ENSO modulates the storm track behavior over western U.S. with a
393 northwest/southwest precipitation dipole (Gershunov and Barnett 1998), as discussed in Section
394 6d. The projected SSTs used in this study emerge from one possible realization of ENSO. How-
395 ever, there is still substantial uncertainty regarding how El Niño will change under global warming
396 (Fedorov and Philander 2000; Guilyardi et al. 2009), which is ~~a source of~~one of the main sources
397 of uncertainty in our results. Capotondi (2013) showed that the diversity of El Niño character-
398 istics in CCSM4 is comparable to what was found in observations, although, as found by Deser
399 et al. (2012c), the overall magnitude of ENSO in CCSM4 is overestimated by ~30% over the
400 preindustrial time period.

401 **6. Results**

402 *a. Mean climatology*

403 Differences in the mean climate of the WUS, as predicted by VR-CESM across time periods,
404 are depicted in Figure 5. Since the character of WUS precipitation has a strong seasonal contrast,
405 changes to mean precipitation (Pr), near-surface temperature (Tavg) and near-surface relative hu-
406 midity (RH) are depicted for what we refer to as the cool season (October to March) and the warm
407 season (April to September).

408 As a result of enhanced GHG concentrations, mean annual ~~near-surface temperature (Tavg)~~
409 Tavg increases by between 1.5 to 3.5 K from hist to mid and between 4 to 7.5 K from hist to
410 end. Despite the large spatial variation in mean seasonal temperatures, the observed differences
411 in mean temperature across time periods are fairly uniform, particularly over the ocean and in
412 coastal regions. Away from the coast, there is a weak gradient in the temperature change field,
413 with the largest increase in temperatures occurring towards the northeast during the cool season
414 and towards the north during the warm season. The ~~increase in temperature is also increases in~~
415 temperature are about 0.5 K and 1.0 K larger during the warm season compared to the cool season
416 for mid and end, respectively.

417 Overall, future RH is constrained closely to hist since it is governed by competing increases
418 in temperature and atmospheric water vapor content. Although RH increases monotonically over
419 the ocean in response to increased evaporation, over land the character is more heterogeneous:
420 In general, RH tends to increase in regions where Tavg increase is constrained below ~ 2 K, but
421 decrease when Tavg anomaly exceeds ~ 2 K. The decrease in these regions is on the order of 2%
422 and 3-6%, for mid and end respectively. In fact, trends in RH are spatially consistent with tem-
423 perature increase but opposite in magnitude with a spatial correlation coefficient of approximately

424 0.8. This suggests that continental evaporation and oceanic water vapor transport are insufficient
425 vapor sources when the temperature reaches a certain level, consistent with the observation of
426 Joshi et al. (2008). This effect has also been observedfound in results by Rowell and Jones (2006)
427 over continental and southeastern Europeand, and by Simmons et al. (2010) over low-latitude and
428 midlatitude land areas.

429 In response to these changes to temperature those changes to Tavg and RH, from hist to mid,
430 mean precipitation over the entire study domain exhibited a 0.2-0.6 mm/day increase during the
431 cool season (about 10%). The largest changes were over the northwest, where cool-season pre-
432 cipitation emerges from large-scale patterns (namely, atmospheric rivers and associated storm sys-
433 tems)(Trenberth et al. 2003; Neiman et al. 2008). Over the warm season, where precipitation in
434 the WUS is primarily from convection, the increase was around 0.2 mm/day (about 10%) through
435 the intermountain west and southwest with drying through the northwest (a decrease in mean pre-
436 cipitation of 0.2 mm/day). These trends largely hold and intensify through end (with relatively
437 changes for about 20-30% compared to hist), except in the intermountain west and southwest re-
438 gions where precipitation again falls to historical levels. Statistical significance of these results is
439 depicted in Figure 6.

440 The increase in cool season precipitation in the northwest is largely driven by increased inte-
441 grated vapor transport (IVT) (see Figure 8a,b) during extreme precipitation events. As observed
442 in previous studies, IVT is particularly useful for understanding extreme precipitation events that
443 arise from large-scale meteorological features (Ralph et al. 2004; Leung and Qian 2009; Dettinger
444 2011). IVT is composed of humidity and wind velocity, which are column water vapor content
445 and horizontal wind advection, which could both impacted by the climate change signal, as plot-
446 ted in Figure 8b. Over the eastern Pacific, we observe increases in both water vapor content and
447 wind speed, which are in turn responsible for increases to IVT in the Pacific Northwest. However,

448 over the continent, we see a weakening of the westerlies overland driven by a reduced meridional
449 temperature contrast. The increased cool-season IVT does not manifest strongly along the Pacific
450 coast off of California, where IVT is much smaller on average and is primarily modulated by
451 ENSO.

452 Changes in precipitation over the intermountain west and southwest during the warm season are
453 primarily associated with convective processes and so are directly impacted by variations in RH.
454 As shown in Figure 5, RH increases through mid-century in this region (although with modest
455 significance) and then significantly decreases through end-of-century over most the study area
456 (except over where soil moisture was already low in hist). This results in a modest increase in
457 precipitation through mid-century followed by a return to historical precipitation amounts by end-
458 of-century. Further climate warming is expected to further decrease RH and drive increased aridity
459 in this region.

460 *b. Precipitation indices*

461 We now analyze observed changes to the precipitation indices. In this main part, the changes of
462 precipitation characters are analyzed in the aspects of the predefined indices (as given in Table
463 1). For each index, the change for each period, changes from past to future, as yearly averaged
464 over different time periods for all ensemble members, are plotted in Figure 6 (for the indices
465 that quantify precipitation days) and Figure 7 (for the indices describing precipitation-precipitated
466 water amounts).

467 On comparing hist and mid, it is clear that the number of rainy days and frequency of non-
468 extreme precipitation events (≤ 10 mm/day) have has increased significantly (about 10-15%) over
469 the southwest and intermountain west, which is less obvious between mid and end. On the con-
470 trary, the frequency of non-extreme precipitation has decreased significantly over the northwest

471 region and the eastern areas of the Montana, Wyoming, and Oregon (by about 10%). The increase
472 in the frequency of these non-extreme precipitation events ~~explain~~explains the observed change to
473 mean precipitation exhibited in Figure 5, and are largely associated with warm season mesoscale
474 storm systems.

475 Although essentially all regions exhibit an increase in the ~~extreme precipitation~~high-rainy events
476 ($\text{Pr} \geq 10 \text{ mm/day}$), this increase is only statistically significant through the intermountain west
477 and in the Pacific ~~northwest~~Northwest (for $\text{Pr} \geq 20 \text{ mm/day}$). When comparing mid to end,
478 there is a clear and significant increase in extreme precipitation events over the northwest coast
479 ($\sim 20\text{-}30\%$) and eastern flank of the Cascades ($> 40\%$). ~~This result is consistent with the result of~~
480 ~~Dominguez et al. (2012)~~, who observe a robust increase in winter precipitation extremes toward
481 ~~the latter half of the 21st century with an ensemble of RCMs~~. The increase in the northwest
482 is accompanied by a decrease in non-extreme precipitation days, as shown above, indicative of
483 drying over the warm season. The positive signal of changes in winter precipitation extremes is
484 also observed in~~Dominguez et al. (2012) but over entire west U.S. in the aspect of return levels~~
485 toward the latter half of the 21st century using an ensemble of RCMs.

486 ~~Notably, our results show~~Notably, no significant changes in mean precipitation or precipitation
487 extremes are predicted for California. In fact, the precipitation signal under a warmer climate is
488 more ambiguous for California (Neelin et al. 2013) in light of the extreme ~~variability of the region~~
489 ~~on interannual time scales (Dettinger 2011)~~. interannual variability (Dettinger 2011). Our results
490 show a small decrease in extreme precipitation over the Sierra Nevada (although the decrease is
491 not statistically significant). On the contrary, Kim (2005) found that under global warming, heavy
492 precipitation events increase in ~~frequency in~~ the mountainous regions of the northern California
493 Coastal Range and the Sierra Nevada. ~~However, our results show a small decrease in extreme~~
494 ~~precipitation over the Sierra Nevada (although the decrease is not statistically significant)~~. This

495 leads us to the likely conclusion (particularly in light of VR-CESM's own biases in this region)
496 that projections in this region are highly dependent on model formulation and the representation
497 of the large-scale circulation patterns effects particularly ENSO as further discussed in the Section

498 **6d.**

499 For the most extreme precipitation events ($\text{Pr} \geq 40 \text{ mm/day}$), there is a statistically signifi-
500 cant increase along the northwest coast ($\geq 60\%$), the Cascades ($\sim 50\%$) and Northern Rockies (\geq
501 60%) by end-of-century. Significant increases are also apparent along the Klamath range in Cal-
502 ifornia of about 20-40% from hist to end. Changes in accumulated precipitation for these events
503 (see Figure 7) are consistent with the change in their frequency(see Figure 7). With a projected
504 increase amplification of temperatures in this region these regions of 4-5 K over the cool season,
505 this increase of precipitation extremes is in excess of the 7% per degree change that would be an-
506 ticipated from the C-C relationship(Figure 8a). In this case, the probable cause of this excess is due
507 to the intensification of the storm track along the coast discussed in section as further discussed in
508 Section 6a.

509 *c. Regional precipitation frequency distributions*

510 To further investigate the regional heterogeneity of changing precipitation, frequency distribu-
511 tions of daily rainfall for rainy daysbased on the days (with $\text{Pr} \geq 0.1 \text{ mm/day}$) are plotted in Figure
512 9 for (a) the Pacific northwestNorthwest, including Washington and Oregon, (b) central and south-
513 ern California, (c) the intermountain west, including Nevada and Utah and (d) the southwest,
514 including Arizona and New Mexico. Frequency plots are developed using simulation outputs at
515 all grid points within each region. Results here mirror our earlier discussion. Over the northwest,
516 precipitation intensity increases with a shift towards a greater frequency of the most extreme pre-
517 cipitation days, especially by end-of-century, accompanied by a reduction in non-extreme precipi-

518 tation days. No significant shifts can be observed for the California region. Over the intermountain
519 west, there is a similar trend towards more extreme precipitation as in the northwest, but with no
520 reduction in warm season non-extreme precipitation days. ~~Finally, in As for~~ the southwest, pre-
521 cipitation is more frequent, but the response is weaker than that observed in the intermountain
522 west.

523 As a supplement, the 95th percentile (P95) based on all days over each simulation period is
524 given in Figure 10 for a more clear understanding of how the most extreme precipitation events
525 are changing. Again, the shift to more extreme precipitation is most pronounced as warming
526 intensifies through the end of the 21st century over the northwest U.S. (P95 increased for about
527 20-30%). For dry regions, including the southwest and intermountain west, precipitation tends to
528 be more extreme (P95 increased for about 15%) with the increase of both the mean precipitation
529 and number of rainy days (see Figure 6) from hist to mid. However, this trend is suppressed when
530 the warming persists till the end over southern California and remaining southwest area where
531 convective precipitation dominates, due to the insufficient compensation of air water vapor to the
532 exponentially enlarged saturated vapor pressure.

533 *d. Disentangling the direct climate signal from ENSO and PDO*

534 As discussed earlier, this study assumes a fixed pattern of SSTs that is consistent across all
535 ensemble members and incorporates certain assumptions on the character of ENSO through the
536 end-of-century that arise from the coupled model. The phase of ENSO is well known to have
537 important repercussions for precipitation extremes (Larkin and Harrison 2005; Allan and Soden
538 2008; Maloney et al. 2014; Yoon et al. 2015). In particular, Cai et al. (2014) found a significant
539 increase in extraordinary precipitation events through the eastern Pacific Ocean in the 21st century
540 within the CMIP5 ensemble, associated with increasing frequency of extreme El Niño events due

541 to greenhouse warming. To better understand how ENSO has impacted our results, we now turn
542 our attention to understanding how precipitation extremes behave in response to the phase of
543 ENSO.

544 In our study, mean SSTs over the Niño 3.4 region are 26.83, 28.62 and 30.54°C for hist, mid and
545 end respectively. Based on the ONI index values, the mean SST anomalies over Niño 3.4 region
546 are 1.38, 1.71 and 2.30 K during El Niño years, and -1.16, -1.62 and -1.43 K during La Niña years,
547 again for hist, mid and end. It is apparent ~~within~~ that within this dataset the magnitude of SST
548 anomalies associated with [the warm phase of ENSO](#) has intensified. ~~Spatial~~ [The spatial](#) pattern of
549 SST anomalies averaged over the warm and cool phases of ENSO can be found in the supplement
550 Figure [S5](#), [suggesting S7](#). [The calculated ONI index values suggest](#) an increasing frequency of El
551 Niño through mid and an almost doubled frequency of La Niña during mid and end compared to
552 the hist ([see the supplement Figure S4](#)).

553 Differences in mean precipitation and associated indices taken between the warm phase (i.e.
554 El Niño) and cool phase (i.e. La Niña) of ENSO are provided in Figure 11 for the cool seasons
555 from hist, mid and end. During the El Niño phase, intensified mean precipitation is expected
556 over California and the southwest (Hamlet and Lettenmaier 2007), accompanied by reduced pre-
557 cipitation intensity over the northwest. In the La Niña phase, this pattern is reversed, with wetter
558 conditions in the northwest and a drier southwest. Consequently, ENSO is associated with a
559 northwest/southwest precipitation dipole, triggered by ENSO's modification of the storm track
560 (Gershunov and Barnett 1998; Leung et al. 2003b), along with modulation of the enhanced pre-
561 cipitation variability (Cayan et al. 1999; Kahya and Dracup 1994). [The dipole effect intensifies](#)
562 [as a compound result of the climate warming effect and the changed magnitude of the ENSO](#)
563 [anomalies](#). Strengthening storm patterns associated with ENSO are also found by Maloney et al.

564 (2014) over California using CMIP5 output under RCP8.5. This dipole is also apparent in the
565 frequency of rainy days and extreme precipitation events.

566 The impact of ENSO can also be seen in the IVT difference that arises between El Niño and
567 La Niña phases in each time period (see Figure 12) and the accompanying 850 hPa wind patterns.
568 During the El Niño phase, there is an increase in on-shore moisture flux over California that
569 triggers a returning circulation through the northwest. This suggests that understanding moisture
570 flux regulation from ENSO is a very important contributor to the character of future precipitation
571 extremes.

572 Based on the above results, it is apparent that the magnitude of the effects of ENSO is compa-
573 rable or even higher than the impacts of climate forcing – that is, shifts in the future character of
574 ENSO would have more dire implications for precipitation extremes than shifts in mean climato-
575 logical forcing. To investigate this further, linear regression has applied at each grid point using
576 a simple linear model that incorporates the phase of ENSO (using the Niño 3.4 SST anomaly)
577 and the underlying climate forcing yearly (from mean GHG concentration). The precipitation in-
578 dices are used as response variables. The significance of these two factors was then obtained from
579 ANOVA (analysis of variance) output (see the supplement Figure S6S8). The magnitude of the
580 response associated with each factor was also computed (see the supplement Figure S7S9). As
581 expected, the ENSO forcing matches most closely with the difference between El Niño and La
582 Niña (see Figure 12). Hence, we observe that ENSO is a major driver of precipitation character
583 through California, the intermountain west, and the southwest and does have an impact on mean
584 precipitation through the Cascades. In contrast, the impacts of climate forcing are visually similar
585 to the pattern of the difference between the different time periods (see Figure 6), and primarily
586 impacts both extreme and non-extreme precipitation in the northwest and intermountain west.

587 We have also assessed the impacts of the Pacific Decadal Oscillation (PDO) on precipitation and
588 observed only a weak correlation between the PDO pattern and precipitation. That is, precipita-
589 tion features did not change substantially between the cool phase or warm phase of PDO when
590 examining ~~hist data~~historical simulations. However, when in phase with ENSO, PDO did have
591 an observable impact over the northwest. This coupled effect has been found by studies such as
592 Gershunov and Barnett (1998), who observed that ENSO and PDO can “reinforce” each other,
593 with PDO responding to the same internal atmospheric variability as ENSO (Pierce 2002). In our
594 simulations, there were roughly an equal number of positive ~~PDO years~~ and negative PDO years in
595 the data from each time period, ~~but since~~. Since SSTs were fixed among ensemble members, the
596 26 year simulation period might be insufficient to account for the variability of PDO. Therefore,
597 in this study, we draw no conclusions on the impact of PDO.

598 7. Discussion and Summary

599 In this study, an ensemble of 26-year simulations ~~have~~has been conducted using VR-CESM with
600 the finest local grid resolution of $\sim 0.25^\circ$ to assess the changing character of precipitation over the
601 21st ~~Century~~century in the WUS. Climate forcing for future projections is prescribed under the
602 ~~RCP8.5~~RCP 8.5 “business-as-usual” scenario. What we found in this study is generally consistent
603 with previous studies’ results about the changing trend of precipitation over the 21st century
604 using CMIP5 simulations (Sillmann et al. 2013b). However, our work provides significantly more
605 regional details with crucial enhancement of precipitation representations, especially over complex
606 terrains.

607 Evaluated against historical ~~reanalysis and gridded~~gridded observations and reanalysis data,
608 VR-CESM was found to accurately capture the spatial patterns of precipitation, including
609 ~~precipitation its~~ frequency and intensity, ~~although it exhibited~~though exhibiting an overestimation

610 of precipitation over the eastern flank of the Cascades, throughout California's Central Valley and
611 along the Sierra Nevada. Nonetheless, there was ~~clear-pronounced~~ improvement in the represen-
612 tation of precipitation features when compared with coarse ~~resolution simulations ($\sim 1^\circ$ resolution~~
613 ~~simulations~~°).

614 ~~Both mean changes to precipitation and~~ Not only mean precipitation but also distributions of
615 both non-extreme and extreme ~~events, precipitation events have been investigated, as~~ projected
616 by the VR-CESM model under climate forcing, ~~have been investigated~~. Although constrained by
617 water influx and soil moisture, changes ~~to in~~ extreme precipitation are hypothesized to follow the
618 C-C relationship more closely than total precipitation amount ($\sim 7\%$ per degree K). In general,
619 this only seemed to be the case over the intermountain west; the northwest exhibited an enhanced
620 response from extreme precipitation ($\sim 10\%$ per degree K), whereas California and the southwest
621 observed essentially no response.

622 From the VR-CESM results, the warming response to the ~~RCP8.5~~ RCP 8.5 climate forcing ex-
623 hibited roughly uniform character, although warming was more pronounced away from the coast
624 and to the north. ~~Future~~ In the future, relative humidity (RH) was ~~observed projected~~ to be con-
625 strained by competing increases in both temperature and atmospheric water vapor content. RH
626 tended to increase in regions where average temperature increase was below ~ 2 K, and decrease
627 when average temperature increase exceeded ~ 2 K. This suggests that continental evaporation
628 and oceanic water vapor transport are insufficient vapor sources to maintain RH levels above a
629 certain threshold temperature. In response, mean precipitation increase is fairly inhomogeneous,
630 with a more pronounced increase in the ~~Northwest where~~ northwest where water vapor transport
631 is ~~enhanced~~ largely enhanced.

632 Over the intermountain west and southwest, an increase in warm season RH through mid-century
633 led to a statistically significant increase in precipitation and non-extreme rainy days due to in-

634 creased convection. This increase levels off through end-of-century, when ~~increased temperatures~~
635 ~~are continuing warming is~~ observed to drive a reduction in RH. Nonetheless, there is a significant
636 increase in extreme precipitation episodes ($\geq \text{Pr} > 10 \text{ mm/day}$) over the intermountain west which
637 is not observed in the southwest.

638 Over the northwest, there is a clear shift from non-extreme precipitation events to extreme pre-
639 cipitation events associated with a moistening of the cool ~~season~~ ~~seasons~~ and drying through the
640 warm season. ~~Although seasons. Specifically, although~~ the total number of annual precipitation
641 days remains relatively constant, ~~there is a decrease in < 10 mm/day precipitation days and an~~
642 ~~increase in > 20 mm/day precipitation days~~ low-rainy days tend to decrease and heavy-rainy days
643 are projected to increase. In each case, the change is on the order of 10 days/year. ~~This change~~ The
644 increase of heavy precipitation frequency is driven by ~~the~~ increased IVT over the eastern Pacific,
645 ~~associated in association~~ with atmospheric river (AR) episodes. ~~Increased~~, and intensified drying
646 over the warm season is ~~driven caused~~ by a reduction in RH. ~~Increased~~ The more frequent cool
647 season precipitation extremes in this region tend to result in ~~high~~ ~~higher~~ runoff events, which are
648 in turn associated with a greater chance of flooding, particularly from rain-on-snow events.

649 Over California, except along the northernmost coast, there is no ~~clear climate signal apparent~~
650 ~~apparent climate signal~~ in the mean precipitation or extremes. Interannual variability in this region
651 associated with ENSO dominates precipitation patterns throughout the historical period and the
652 21st century. ENSO drives precipitation behavior by modulating the ~~midlatitudinal~~ ~~mid-latitudinal~~
653 storm track in this region. In particular, during the El Niño phase, there is an increase in on-
654 shore moisture flux over California that triggers a returning circulation through the northwest.
655 The results over California highlight the importance of understanding the response of ENSO to
656 climate change (which is still largely inconsistent in CMIP5 climate models and so is a key source

657 of uncertainty in our results), since variations in the magnitude or structure of ENSO will have
658 immediate consequences for precipitation in this region.

659 The projected SSTs utilized for this study through end-of-century suggest that SST anomalies
660 associated with ENSO will intensify. The impacts of ENSO are wide-reaching, with a statis-
661 tically significant response observed in the character of precipitation throughout California, the
662 intermountain west and the southwest regions, as well as impacting mean precipitation through
663 the Cascades. In contrast, the significance of climate forcing (when compensating for ENSO)
664 largely matched the differences observed between time periods, and had its greatest impact on
665 both extreme and non-extreme precipitation in the northwest and intermountain west.

666 *Acknowledgments.* The authors would like to thank Michael Wehner for sharing the 0.25°
667 uniform-resolution CESM dataset ~~, and his many and his helpful~~ suggestions. The authors also
668 want to thank Alan M. Rhoades for providing part of the simulation output and ~~providing sharing~~
669 his feedback on the manuscript. We acknowledge the substantial efforts behind the datasets used
670 in this study, including UW, NCDC, and NARR. The simulation ~~data used dataset used in this~~
671 study is available by request at xyhuang@ucdavis.edu. This project is supported in part by the
672 University of California, Davis and by the Department of Energy “Multiscale Methods for Accu-
673 rate, Efficient, and Scale-Aware Models of the Earth System” project. Support also comes from
674 the California Agricultural Experiment Station (project CA-D-LAW-2203-H).

675 References

- 676 AchutaRao, K., and K. R. Sperber, 2006: ENSO simulation in coupled ocean-atmosphere
677 models: are the current models better? *Climate Dynamics*, **27** (1), 1–15, doi:10.1007/
678 s00382-006-0119-7.

- 679 Alexander, L., and Coauthors, 2006: Global observed changes in daily climate extremes of temper-
680 ature and precipitation. *Journal of Geophysical Research: Atmospheres (1984–2012)*, **111** (D5),
681 doi:10.1029/2005JD006290.
- 682 Allan, R. P., and B. J. Soden, 2008: Atmospheric warming and the amplification of precipitation
683 extremes. *Science*, **321** (5895), 1481–1484, doi:10.1126/science.1160787.
- 684 Allen, M. R., and W. J. Ingram, 2002: Constraints on future changes in climate and the hydrologic
685 cycle. *Nature*, **419** (6903), 224–232, doi:10.1038/nature01092.
- 686 Ashfaq, M., D. Rastogi, R. Mei, S.-C. Kao, S. Gangrade, B. Naz, and D. Touma, 2016: High-
687 resolution ensemble projections of near-term regional climate over the continental United States.
688 *Journal of Geophysical Research: Atmospheres*, doi:10.1002/2016JD025285.
- 689 Bell, J. L., L. C. Sloan, and M. A. Snyder, 2004: Regional changes in extreme climatic events:
690 a future climate scenario. *Journal of Climate*, **17** (1), 81–87, doi:10.1175/1520-0442(2004)
691 017<0081:RCIECE>2.0.CO;2.
- 692 Cai, W., and Coauthors, 2014: Increasing frequency of extreme El Niño events due to greenhouse
693 warming. *Nature Climate Change*, **4** (2), 111–116, doi:10.1038/nclimate2100.
- 694 Caldwell, P., 2010: California wintertime precipitation bias in regional and global climate
695 models. *Journal of Applied Meteorology and Climatology*, **49** (10), 2147–2158, doi:10.1175/
696 2010JAMC2388.1.
- 697 Capotondi, A., 2013: ENSO diversity in the NCAR CCSM4 climate model. *Journal of Geophysi-
698 cal Research: Oceans*, **118** (10), 4755–4770, doi:10.1002/jgrc.20335.

- 699 Cayan, D. R., T. Das, D. W. Pierce, T. P. Barnett, M. Tyree, and A. Gershunov, 2010: Future
700 dryness in the southwest US and the hydrology of the early 21st century drought. *Proceedings*
701 *of the National Academy of Sciences*, **107** (50), 21 271–21 276, doi:10.1073/pnas.0912391107.
- 702 Cayan, D. R., K. T. Redmond, and L. G. Riddle, 1999: ENSO and hydrologic extremes in the
703 western United States. *Journal of Climate*, **12** (9), 2881–2893, doi:10.1175/1520-0442(1999)
704 012<2881:EAHEIT>2.0.CO;2.
- 705 Collins, M., and Coauthors, 2010: The impact of global warming on the tropical Pacific Ocean
706 and El Niño. *Nature Geoscience*, **3** (6), 391–397, doi:10.1038/ngeo868.
- 707 Dennis, J., and Coauthors, 2011: CAM-SE: A scalable spectral element dynamical core for the
708 Community Atmosphere Model. *International Journal of High Performance Computing Appli-*
709 *cations*, 1094342011428142, doi:10.1177/1094342011428142.
- 710 Deser, C., R. Knutti, S. Solomon, and A. S. Phillips, 2012a: Communication of the role of natural
711 variability in future North American climate. *Nature Climate Change*, **2** (11), 775–779, doi:
712 10.1038/nclimate1562.
- 713 Deser, C., A. Phillips, V. Bourdette, and H. Teng, 2012b: Uncertainty in climate change pro-
714 jections: the role of internal variability. *Climate Dynamics*, **38** (3-4), 527–546, doi:10.1007/
715 s00382-010-0977-x.
- 716 Deser, C., and Coauthors, 2012c: ENSO and Pacific decadal variability in the Community
717 Climate System Model version 4. *Journal of Climate*, **25** (8), 2622–2651, doi:10.1175/
718 JCLI-D-11-00301.1.

- 719 Dettinger, M., 2011: Climate change, atmospheric rivers, and floods in California—a mul-
720 timodel analysis of storm frequency and magnitude changes. Wiley Online Library, doi:
721 10.1111/j.1752-1688.2011.00546.x.
- 722 Diffenbaugh, N. S., J. S. Pal, R. J. Trapp, and F. Giorgi, 2005: Fine-scale processes regulate the re-
723 sponse of extreme events to global climate change. *Proceedings of the National Academy of Sci-*
724 *ences of the United States of America*, **102** (44), 15 774–15 778, doi:10.1073/pnas.0506042102.
- 725 DiNezio, P. N., B. P. Kirtman, A. C. Clement, S.-K. Lee, G. A. Vecchi, and A. Wittenberg, 2012:
726 Mean climate controls on the simulated response of ENSO to increasing greenhouse gases.
727 *Journal of Climate*, **25** (21), 7399–7420, doi:10.1175/JCLI-D-11-00494.1.
- 728 Dominguez, F., E. Rivera, D. Lettenmaier, and C. Castro, 2012: Changes in winter precipitation
729 extremes for the western United States under a warmer climate as simulated by regional climate
730 models. *Geophysical Research Letters*, **39** (5), doi:10.1029/2011GL050762.
- 731 Donat, M. G., A. L. Lowry, L. V. Alexander, P. A. OGorman, and N. Maher, 2016: More ex-
732 treme precipitation in the world’s dry and wet regions. *Nature Climate Change*, doi:10.1038/
733 *nclimate2941*.
- 734 Duffy, P., and Coauthors, 2006: Simulations of present and future climates in the western United
735 States with four nested regional climate models. *Journal of Climate*, **19** (6), 873–895, doi:
736 10.1175/JCLI3669.1.
- 737 Duli  re, V., Y. Zhang, and E. P. Salath   Jr, 2011: Extreme precipitation and temperature over
738 the US Pacific Northwest: A comparison between observations, reanalysis data, and regional
739 models. *Journal of Climate*, **24** (7), 1950–1964, doi:10.1175/2010JCLI3224.1.

- 740 Easterling, D. R., G. A. Meehl, C. Parmesan, S. A. Changnon, T. R. Karl, and L. O. Mearns, 2000:
741 Climate extremes: observations, modeling, and impacts. *Science*, **289** (5487), 2068–2074, doi:
742 10.1126/science.289.5487.2068.
- 743 Fedorov, A. V., and S. G. Philander, 2000: Is El Niño changing? *Science*, **288** (5473), 1997–2002,
744 doi:10.1126/science.288.5473.1997.
- 745 Fox-Rabinovitz, M., J. Côté, B. Dugas, M. Déqué, and J. L. McGregor, 2006: Variable resolution
746 general circulation models: Stretched-grid model intercomparison project (SGMIP). *Journal of*
747 *Geophysical Research: Atmospheres (1984–2012)*, **111** (D16), doi:10.1029/2005JD006520.
- 748 Fox-Rabinovitz, M. S., G. L. Stenchikov, M. J. Suarez, and L. L. Takacs, 1997: A finite-
749 difference GCM dynamical core with a variable-resolution stretched grid. *Monthly Weather
750 Review*, **125** (11), 2943–2968, doi:10.1175/1520-0493(1997)125<2943:AFDGDC>2.0.CO;2.
- 751 Frei, C., R. Schöll, S. Fukutome, J. Schmidli, and P. L. Vidale, 2006: Future change of precipita-
752 tion extremes in Europe: Intercomparison of scenarios from regional climate models. *Journal
753 of Geophysical Research: Atmospheres (1984–2012)*, **111** (D6), doi:10.1029/2005JD005965.
- 754 Gao, Y., J. Lu, L. R. Leung, Q. Yang, S. Hagos, and Y. Qian, 2015: Dynamical and thermody-
755 namical modulations on future changes of landfalling atmospheric rivers over western North
756 America. *Geophysical Research Letters*, **42** (17), 7179–7186, doi:10.1002/2015GL065435.
- 757 Gates, W. L., 1992: AMIP: The Atmospheric Model Intercomparison Project. *Bulletin of the
758 American Meteorological Society*, **73**, 1962–1970.
- 759 Gershunov, A., and T. P. Barnett, 1998: Interdecadal modulation of ENSO teleconnec-
760 tions. *Bulletin of the American Meteorological Society*, **79** (12), 2715–2725, doi:10.1175/
761 1520-0477(1998)079<2715:IMOET>2.0.CO;2.

- 762 Gettelman, A., H. Morrison, and S. J. Ghan, 2008: A new two-moment bulk stratiform cloud
763 microphysics scheme in the Community Atmosphere Model, version 3 (CAM3). Part II:
764 Single-column and global results. *Journal of Climate*, **21** (15), 3660–3679, doi:10.1175/
765 2008JCLI2116.1.
- 766 Grodsky, S. A., J. A. Carton, S. Nigam, and Y. M. Okumura, 2012: Tropical Atlantic biases in
767 CCSM4. *Journal of Climate*, **25** (11), 3684–3701, doi:10.1175/JCLI-D-11-00315.1.
- 768 Guilyardi, E., A. Wittenberg, A. Fedorov, M. Collins, C. Wang, A. Capotondi, G. J. Van Old-
769 enborgh, and T. Stockdale, 2009: Understanding El Niño in ocean-atmosphere general cir-
770 culation models. *Bulletin of the American Meteorological Society*, **90** (3), 325, doi:10.1175/
771 2008BAMS2387.1.
- 772 Hamlet, A. F., and D. P. Lettenmaier, 2005: Production of temporally consistent gridded precip-
773 itation and temperature fields for the continental United States. *Journal of Hydrometeorology*,
774 **6** (3), 330–336, doi:10.1175/JHM420.1.
- 775 Hamlet, A. F., and D. P. Lettenmaier, 2007: Effects of 20th century warming and climate
776 variability on flood risk in the western US. *Water Resources Research*, **43** (6), doi:10.1029/
777 2006WR005099.
- 778 Hegerl, G. C., F. W. Zwiers, P. A. Stott, and V. V. Kharin, 2004: Detectability of anthropogenic
779 changes in annual temperature and precipitation extremes. *Journal of Climate*, **17** (19), 3683–
780 3700, doi:10.1175/1520-0442(2004)017<3683:DOACIA>2.0.CO;2.
- 781 Huang, X., A. M. Rhoades, P. A. Ullrich, and C. M. Zarzycki, 2016: An evaluation of the variable
782 resolution-CESM for modeling California’s climate. *Journal of Advances in Modeling Earth
783 Systems*, doi:10.1002/2015MS000559.

- 784 Huang, X., and P. A. Ullrich, 2016: Irrigation impacts on California's climate with the variable-
785 resolution CESM. *Journal of Advances in Modeling Earth Systems*, **8** (3), 1151–1163, doi:
786 10.1002/2016MS000656.
- 787 Hurrell, J. W., J. J. Hack, D. Shea, J. M. Caron, and J. Rosinski, 2008: A new sea surface temper-
788 ature and sea ice boundary dataset for the Community Atmosphere Model. *Journal of Climate*,
789 **21** (19), 5145–5153, doi:10.1175/2008JCLI2292.1.
- 790 Hurrell, J. W., and Coauthors, 2013: The community earth system model: A framework for col-
791 laborative research. *Bulletin of the American Meteorological Society*, **94** (9), 1339–1360, doi:
792 10.1175/BAMS-D-12-00121.1.
- 793 Jha, B., Z.-Z. Hu, and A. Kumar, 2014: SST and ENSO variability and change simulated in
794 historical experiments of CMIP5 models. *Climate Dynamics*, **42** (7–8), 2113–2124, doi:10.1007/
795 s00382-013-1803-z.
- 796 Joseph, R., and S. Nigam, 2006: ENSO evolution and teleconnections in IPCC's twentieth-century
797 climate simulations: Realistic representation? *Journal of Climate*, **19** (17), 4360–4377, doi:
798 10.1175/JCLI3846.1.
- 799 Joshi, M. M., J. M. Gregory, M. J. Webb, D. M. Sexton, and T. C. Johns, 2008: Mechanisms for
800 the land/sea warming contrast exhibited by simulations of climate change. *Climate Dynamics*,
801 **30** (5), 455–465, doi:10.1007/s00382-007-0306-1.
- 802 Kahya, E., and J. A. Dracup, 1994: The influences of type 1 El Nino and La Nina events on
803 streamflows in the Pacific southwest of the United States. *Journal of Climate*, **7** (6), 965–976,
804 doi:10.1175/1520-0442(1994)007<0965:TIOTEN>2.0.CO;2.

- 805 Kao, H.-Y., and J.-Y. Yu, 2009: Contrasting eastern-Pacific and central-Pacific types of ENSO.
806 *Journal of Climate*, **22** (3), 615–632, doi:10.1175/2008JCLI2309.1.
- 807 Karl, T. R., N. Nicholls, and A. Ghazi, 1999: Clivar/GCOS/WMO workshop on indices and indi-
808 cators for climate extremes workshop summary. *Weather and Climate Extremes*, Springer, 3–7,
809 doi:10.1023/A:1005491526870.
- 810 Kharin, V. V., F. Zwiers, X. Zhang, and M. Wehner, 2013: Changes in temperature and
811 precipitation extremes in the CMIP5 ensemble. *Climatic Change*, **119** (2), 345–357, doi:
812 10.1007/s10584-013-0705-8.
- 813 Kharin, V. V., F. W. Zwiers, X. Zhang, and G. C. Hegerl, 2007: Changes in temperature and
814 precipitation extremes in the IPCC ensemble of global coupled model simulations. *Journal of*
815 *Climate*, **20** (8), 1419–1444, doi:10.1175/JCLI4066.1.
- 816 Kim, J., 2005: A projection of the effects of the climate change induced by increased CO₂ on
817 extreme hydrologic events in the western US. *Climatic Change*, **68** (1-2), 153–168, doi:10.
818 1007/s10584-005-4787-9.
- 819 Laprise, R., and Coauthors, 2008: Challenging some tenets of regional climate modelling. *Meteo-
820 rology and Atmospheric Physics*, **100** (1-4), 3–22, doi:10.1007/s00703-008-0292-9.
- 821 Larkin, N. K., and D. Harrison, 2005: On the definition of El Niño and associated seasonal average
822 US weather anomalies. *Geophysical Research Letters*, **32** (13), doi:10.1029/2005GL022738.
- 823 Latif, M., and N. S. Keenlyside, 2009: El Niño/Southern Oscillation response to global warming.
824 *Proceedings of the National Academy of Sciences*, **106** (49), 20 578–20 583, doi:10.1073/pnas.
825 0710860105.

- 826 Leung, L. R., L. O. Mearns, F. Giorgi, and R. L. Wilby, 2003a: Regional climate research: needs
827 and opportunities. *Bulletin of the American Meteorological Society*, **84** (1), 89–95, doi:10.1175/
828 BAMS-84-1-89.
- 829 Leung, L. R., and Y. Qian, 2009: Atmospheric rivers induced heavy precipitation and flooding in
830 the western US simulated by the WRF regional climate model. *Geophysical Research Letters*,
831 **36** (3), doi:10.1029/2008GL036445.
- 832 Leung, L. R., Y. Qian, and X. Bian, 2003b: Hydroclimate of the western United States based on
833 observations and regional climate simulation of 1981-2000. Part I: Seasonal statistics. *Journal*
834 *of Climate*, **16** (12), 1892–1911, doi:10.1175/1520-0442(2003)016<1892:HOTWUS>2.0.CO;2.
- 835 Maloney, E. D., and Coauthors, 2014: North American climate in CMIP5 experiments: part iii:
836 assessment of twenty-first-century projections. *Journal of Climate*, **27** (6), 2230–2270, doi:
837 10.1175/JCLI-D-13-00273.1.
- 838 Maurer, E., A. Wood, J. Adam, D. Lettenmaier, and B. Nijssen, 2002: A long-term hydrologically
839 based dataset of land surface fluxes and states for the conterminous United States. *Journal of*
840 *Climate*, **15** (22), 3237–3251, doi:10.1175/1520-0442(2002)015<3237:ALTHBD>2.0.CO;2.
- 841 McDonald, A., 2003: Transparent boundary conditions for the shallow-water equations: test-
842 ing in a nested environment. *Monthly Weather Review*, **131** (4), 698–705, doi:10.1175/
843 1520-0493(2003)131<0698:TBCFTS>2.0.CO;2.
- 844 Meehl, G. A., H. Teng, and G. Branstator, 2006: Future changes of El Niño in two global coupled
845 climate models. *Climate Dynamics*, **26** (6), 549–566, doi:10.1007/s00382-005-0098-0.

- 846 Mesinger, F., and K. Veljovic, 2013: Limited area NWP and regional climate modeling: a test
847 of the relaxation vs Eta lateral boundary conditions. *Meteorology and Atmospheric Physics*,
848 **119** (1-2), 1–16, doi:10.1007/s00703-012-0217-5.
- 849 Mesinger, F., and Coauthors, 2006: North American regional reanalysis. *Bulletin of the American*
850 *Meteorological Society*, **87**, 343–360, doi:10.1175/BAMS-87-3-343.
- 851 Min, S.-K., X. Zhang, F. W. Zwiers, and G. C. Hegerl, 2011: Human contribution to more-intense
852 precipitation extremes. *Nature*, **470** (7334), 378–381, doi:10.1038/nature09763.
- 853 Morrison, H., and A. Gettelman, 2008: A new two-moment bulk stratiform cloud microphysics
854 scheme in the Community Atmosphere Model, version 3 (CAM3). Part I: Description and nu-
855 matical tests. *Journal of Climate*, **21** (15), 3642–3659, doi:10.1175/2008JCLI2105.1.
- 856 Neale, R. B., and Coauthors, 2010a: Description of the NCAR community atmosphere model
857 (CAM 5.0). *NCAR Tech. Note NCAR/TN-486+ STR*.
- 858 Neale, R. B., and Coauthors, 2010b: Description of the NCAR Community Atmosphere Model
859 (CAM 5.0). NCAR Technical Note NCAR/TN-486+STR, National Center for Atmospheric Re-
860 search, Boulder, Colorado, 268 pp.
- 861 Neelin, J. D., B. Langenbrunner, J. E. Meyerson, A. Hall, and N. Berg, 2013: California winter
862 precipitation change under global warming in the Coupled Model Intercomparison Project phase
863 5 ensemble. *Journal of Climate*, **26** (17), 6238–6256, doi:10.1175/JCLI-D-12-00514.1.
- 864 Neiman, P. J., F. M. Ralph, G. A. Wick, J. D. Lundquist, and M. D. Dettinger, 2008: Meteo-
865 rological characteristics and overland precipitation impacts of atmospheric rivers affecting the
866 West Coast of North America based on eight years of SSM/I satellite observations. *Journal of*
867 *Hydrometeorology*, **9** (1), 22–47, doi:10.1175/2007JHM855.1.

- 868 NOAA, 2013: Defining El Niño and La Niña. Accessed 2015-
869 08-20, [https://www.climate.gov/news-features/understanding-climate/
870 watching-el-nio-and-la-nia-noaa-adapts-global-warming](https://www.climate.gov/news-features/understanding-climate/watching-el-nio-and-la-nia-noaa-adapts-global-warming).
- 871 O'Brien, T. A., W. D. Collins, K. Kashinath, O. Rübel, S. Byna, J. Gu, H. Krishnan, and P. A.
872 Ullrich, 2016: Resolution dependence of precipitation statistical fidelity in hindcast simulations.
873 *Journal of Advances in Modeling Earth Systems*, **8** (2), 976–990, doi:10.1002/2016MS000671.
- 874 O'Gorman, P. A., and T. Schneider, 2009: The physical basis for increases in precipitation ex-
875 tremes in simulations of 21st-century climate change. *Proceedings of the National Academy of
876 Sciences*, **106** (35), 14 773–14 777, doi:10.1073/pnas.0907610106.
- 877 Oleson, K., and Coauthors, 2010: Technical description of version 4.0 of the Community Land
878 Model (CLM). NCAR Technical Note NCAR/TN-478+STR, National Center for Atmospheric
879 Research, Boulder, Colorado, 257 pp. doi:10.5065/D6FB50WZ.
- 880 Pendergrass, A. G., F. Lehner, B. M. Sanderson, and Y. Xu, 2015: Does extreme precipitation
881 intensity depend on the emissions scenario? *Geophysical Research Letters*, **42** (20), 8767–8774,
882 doi:10.1002/2015GL065854.
- 883 Pierce, D. W., 2002: The role of sea surface temperatures in interactions between ENSO
884 and the North Pacific Oscillation. *Journal of Climate*, **15** (11), 1295–1308, doi:10.1175/1520-0442(2002)015<1295:TROSST>2.0.CO;2.
- 886 Ralph, F. M., P. J. Neiman, and G. A. Wick, 2004: Satellite and CALJET aircraft observations of
887 atmospheric rivers over the eastern North Pacific Ocean during the winter of 1997/98. *Monthly
888 Weather Review*, **132** (7), 1721–1745, doi:10.1175/1520-0493(2004)132<1721:SACAOO>2.0.
889 CO;2.

- 890 Rauscher, S. A., E. Coppola, C. Piani, and F. Giorgi, 2010: Resolution effects on regional climate
891 model simulations of seasonal precipitation over Europe. *Climate dynamics*, **35** (4), 685–711,
892 doi:10.1007/s00382-009-0607-7.
- 893 Rauscher, S. A., T. A. OBrien, C. Piani, E. Coppola, F. Giorgi, W. D. Collins, and P. M. Lawston,
894 2016: A multimodel intercomparison of resolution effects on precipitation: simulations and
895 theory. *Climate Dynamics*, **47** (7-8), 2205–2218, doi:10.1007/s00382-015-2959-5.
- 896 Rauscher, S. A., T. D. Ringler, W. C. Skamarock, and A. A. Mirin, 2013: Exploring a global
897 multiresolution modeling approach using aquaplanet simulations. *Journal of Climate*, **26** (8),
898 2432–2452, doi:10.1175/JCLI-D-12-00154.1.
- 899 Rhoades, A. M., X. Huang, P. A. Ullrich, and C. M. Zarzycki, 2016: Characterizing sierra nevada
900 snowpack using variable-resolution CESM. *Journal of Applied Meteorology and Climatology*,
901 **55** (1), 173–196, doi:10.1175/JAMC-D-15-0156.1.
- 902 Rhoades, A. M., P. A. Ullrich, and C. M. Zarzycki, 2017: Projecting 21st century snowpack
903 trends in western USA mountains using variable-resolution CESM. *Climate Dynamics*, 1–28,
904 doi:10.1007/s00382-017-3606-0.
- 905 Riahi, K., and Coauthors, 2011: RCP 8.5 – A scenario of comparatively high greenhouse gas
906 emissions. *Climatic Change*, **109** (1-2), 33–57, doi:10.1007/s10584-011-0149-y.
- 907 Rowell, D. P., and R. G. Jones, 2006: Causes and uncertainty of future summer drying over Europe.
908 *Climate Dynamics*, **27** (2-3), 281–299, doi:10.1007/s00382-006-0125-9.
- 909 Salathé Jr, E. P., R. Steed, C. F. Mass, and P. H. Zahn, 2008: A high-resolution climate model for
910 the US Pacific Northwest: Mesoscale feedbacks and local responses to climate change. *Journal*
911 *of Climate*, **21** (21), 5708–5726, doi:10.1175/2008JCLI2090.1.

- 912 Scoccimarro, E., M. Zampieri, A. Bellucci, A. Navarra, and Coauthors, 2013: Heavy precipitation
913 events in a warmer climate: Results from CMIP5 models. *Journal of Climate*, doi:10.1175/
914 JCLI-D-12-00850.1.
- 915 Seneviratne, S. I., and Coauthors, 2012: Changes in climate extremes and their impacts on the
916 natural physical environment. *Managing the risks of extreme events and disasters to advance*
917 *climate change adaptation*, 109–230.
- 918 Sillmann, J., V. Kharin, X. Zhang, F. Zwiers, and D. Bronaugh, 2013a: Climate extremes indices
919 in the CMIP5 multimodel ensemble: Part 1. Model evaluation in the present climate. *Journal of*
920 *Geophysical Research: Atmospheres*, **118** (4), 1716–1733, doi:10.1002/jgrd.50203.
- 921 Sillmann, J., V. Kharin, F. Zwiers, X. Zhang, and D. Bronaugh, 2013b: Climate extremes indices
922 in the CMIP5 multimodel ensemble: Part 2. Future climate projections. *Journal of Geophysical*
923 *Research: Atmospheres*, **118** (6), 2473–2493, doi:10.1002/jgrd.50188.
- 924 Simmons, A., K. Willett, P. Jones, P. Thorne, and D. Dee, 2010: Low-frequency variations
925 in surface atmospheric humidity, temperature, and precipitation: Inferences from reanalyses
926 and monthly gridded observational data sets. *Journal of Geophysical Research: Atmospheres*,
927 **115** (D1), doi:10.1029/2009JD012442.
- 928 Singh, D., M. Tsiang, B. Rajaratnam, and N. S. Diffenbaugh, 2013: Precipitation extremes over the
929 continental United States in a transient, high-resolution, ensemble climate model experiment.
930 *Journal of Geophysical Research: Atmospheres*, **118** (13), 7063–7086, doi:10.1002/jgrd.50543.
- 931 Small, R. J., and Coauthors, 2014: A new synoptic scale resolving global climate simulation using
932 the Community Earth System Model. *Journal of Advances in Modeling Earth Systems*, **6** (4),
933 1065–1094, doi:10.1002/2014MS000363.

- 934 Staniforth, A. N., and H. L. Mitchell, 1978: A variable-resolution finite-element technique for
935 regional forecasting with the primitive equations. *Monthly Weather Review*, **106** (4), 439–447,
936 doi:10.1175/1520-0493(1978)106<0439:AVRFET>2.0.CO;2.
- 937 Stephens, G. L., and Coauthors, 2010: Dreary state of precipitation in global models. *Journal of*
938 *Geophysical Research: Atmospheres*, **115** (D24), doi:10.1029/2010JD014532.
- 939 Stevenson, S., 2012: Significant changes to ENSO strength and impacts in the twenty-first century:
940 Results from CMIP5. *Geophysical Research Letters*, **39** (17), doi:10.1029/2012GL052759.
- 941 Sugi, M., and J. Yoshimura, 2004: A mechanism of tropical precipitation change due to
942 CO₂ increase. *Journal of Climate*, **17** (1), 238–243, doi:10.1175/1520-0442(2004)017<0238:
943 AMOTPC>2.0.CO;2.
- 944 Taschetto, A. S., A. S. Gupta, N. C. Jourdain, A. Santoso, C. C. Ummenhofer, and M. H. England,
945 2014: Cold tongue and warm pool ENSO events in CMIP5: mean state and future projections.
946 *Journal of Climate*, **27** (8), 2861–2885, doi:10.1175/JCLI-D-13-00437.1.
- 947 Taylor, M. A., 2011: Conservation of mass and energy for the moist atmospheric primitive equa-
948 tions on unstructured grids. *Numerical Techniques for Global Atmospheric Models*, Springer,
949 357–380, doi:10.1007/978-3-642-11640-7_12.
- 950 Tebaldi, C., K. Hayhoe, J. M. Arblaster, and G. A. Meehl, 2006: Going to the extremes. *Climatic*
951 *Change*, **79** (3-4), 185–211, doi:10.1007/s10584-006-9051-4.
- 952 Trenberth, K. E., 2011: Changes in precipitation with climate change. *Climate Research*, **47** (1),
953 123, doi:10.3354/cr00953.

- 954 Trenberth, K. E., A. Dai, R. M. Rasmussen, and D. B. Parsons, 2003: The changing character of
955 precipitation. *Bulletin of the American Meteorological Society*, **84** (9), 1205–1217, doi:10.1175/
956 BAMS-84-9-1205.
- 957 Ullrich, P. A., D. Devendran, and H. Johansen, 2016: Arbitrary-order conservative and consistent
958 remapping and a theory of linear maps, part 2. *Monthly Weather Review*, **144** (4), 1529–1549,
959 doi:10.1175/MWR-D-15-0301.1.
- 960 Ullrich, P. A., and M. A. Taylor, 2015: Arbitrary-order conservative and consistent remapping
961 and a theory of linear maps: Part I. *Monthly Weather Review*, **143** (6), 2419–2440, doi:10.1175/
962 MWR-D-14-00343.1.
- 963 Walker, M. D., and N. S. Diffenbaugh, 2009: Evaluation of high-resolution simulations of daily-
964 scale temperature and precipitation over the United States. *Climate Dynamics*, **33** (7-8), 1131–
965 1147, doi:10.1007/s00382-009-0603-y.
- 966 Wehner, M. F., 2013: Very extreme seasonal precipitation in the NARCCAP ensemble:
967 model performance and projections. *Climate Dynamics*, **40** (1-2), 59–80, doi:10.1007/
968 s00382-012-1393-1.
- 969 Wehner, M. F., R. L. Smith, G. Bala, and P. Duffy, 2010: The effect of horizontal resolution
970 on simulation of very extreme US precipitation events in a global atmosphere model. *Climate
971 Dynamics*, **34** (2-3), 241–247, doi:10.1007/s00382-009-0656-y.
- 972 Wehner, M. F., and Coauthors, 2014: The effect of horizontal resolution on simulation quality in
973 the Community Atmospheric Model, CAM5.1. *Journal of Advances in Modeling Earth Systems*,
974 doi:10.1002/2013MS000276.

- 975 Yoon, J.-H., S. S. Wang, R. R. Gillies, B. Kravitz, L. Hipps, and P. J. Rasch, 2015: Increasing
976 water cycle extremes in California and in relation to ENSO cycle under global warming. *Nature*
977 *Communications*, **6**, doi:10.1038/ncomms9657.
- 978 Zarzycki, C. M., C. Jablonowski, and M. A. Taylor, 2014: Using variable-resolution meshes
979 to model tropical cyclones in the Community Atmosphere Model. *Monthly Weather Review*,
980 **142** (3), 1221–1239, doi:10.1175/MWR-D-13-00179.1.
- 981 Zarzycki, C. M., C. Jablonowski, D. R. Thatcher, and M. A. Taylor, 2015: Effects of localized grid
982 refinement on the general circulation and climatology in the Community Atmosphere Model.
983 *Journal of Climate*, **28** (7), 2777–2803, doi:10.1175/JCLI-D-14-00599.1.
- 984 Zhang, X., L. Alexander, G. C. Hegerl, P. Jones, A. K. Tank, T. C. Peterson, B. Trewin, and
985 F. W. Zwiers, 2011: Indices for monitoring changes in extremes based on daily temperature
986 and precipitation data. *Wiley Interdisciplinary Reviews: Climate Change*, **2** (6), 851–870, doi:
987 10.1002/wcc.147.
- 988 Zhang, X., J. Wang, F. W. Zwiers, and P. Y. Groisman, 2010: The influence of large-scale climate
989 variability on winter maximum daily precipitation over North America. *Journal of Climate*,
990 **23** (11), 2902–2915, doi:10.1175/2010JCLI3249.1.

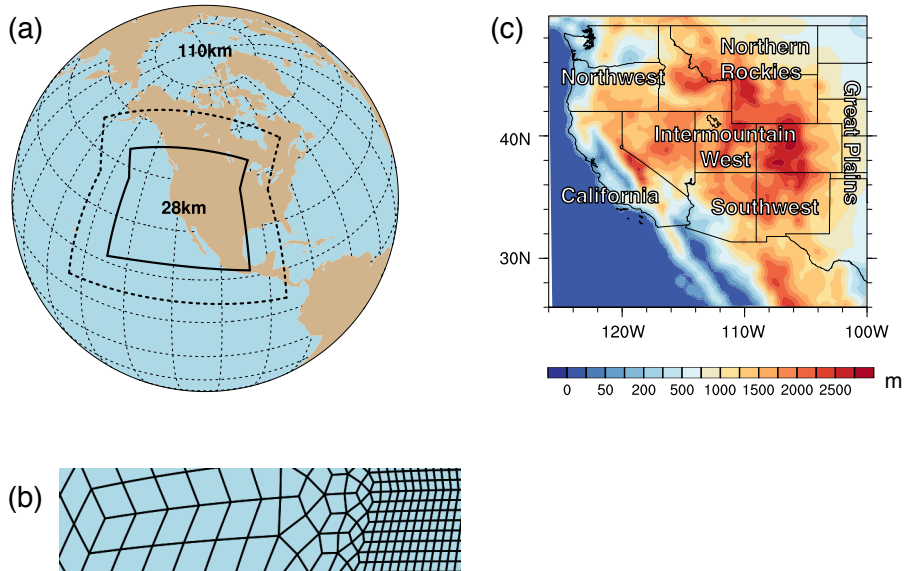
991 LIST OF TABLES

TABLE 1. Precipitation indices employed in this study.

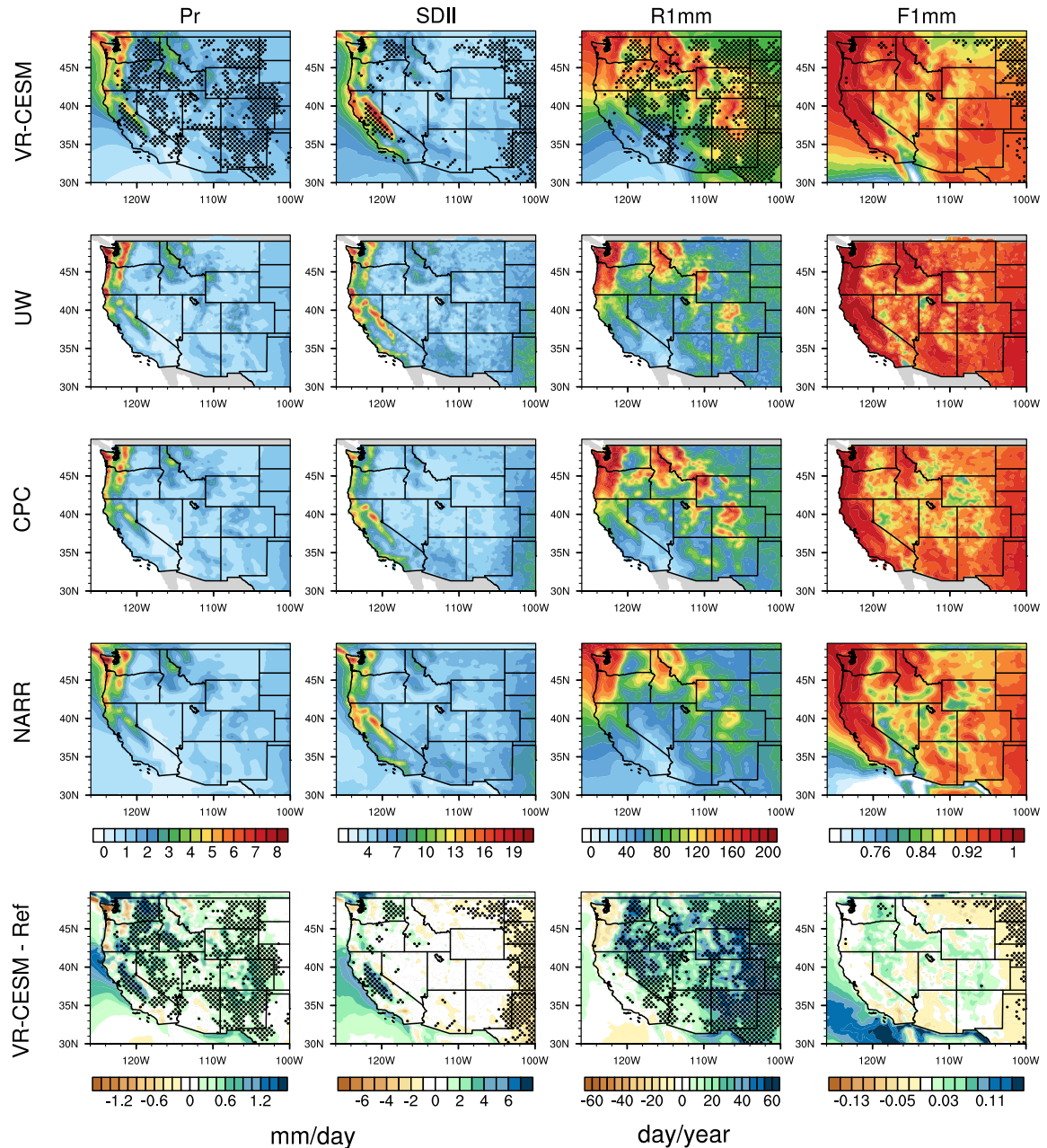
Indice	Definition
Pr	Mean daily precipitation
R1mm	Number of days per year with Pr>1 mm
SDII	Simple precipitation intensity index: Precipitation amount / (R1mm) (mm/day)
R5mm	Number of days per year with Pr>1 mm and Pr= \leq 5 mm
R10mm	Number of days per year with Pr>5 mm and Pr= \leq 10 mm
R20mm	Number of days per year with Pr>10 mm and Pr= \leq 20 mm
R40mm	Number of days per year with Pr>20 mm and Pr= \leq 40 mm
Rxmm	Number of days per year with Pr>40 mm
F1mm	Fraction of precipitation contributed to the total precipitation for days of R1mm (similarly for F5mm, F10mm, F20mm, F40mm and Fxmm)
P5mm	Precipitation amount from R5mm (similarly for P10mm, P20mm, F40mm <u>P40mm</u> , Pxmm)

993 LIST OF FIGURES

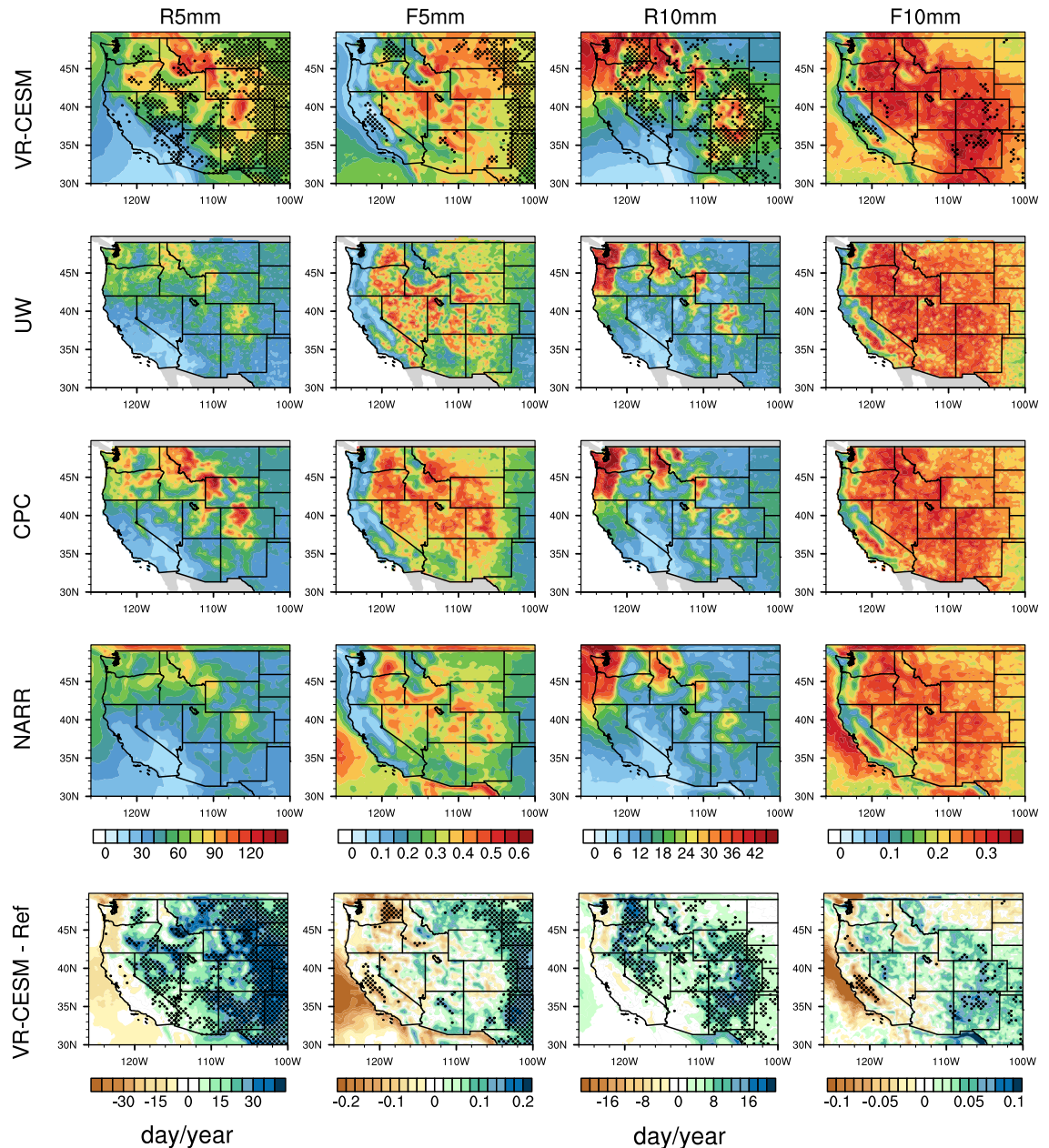
994 Fig. 1.	(a) The approximate grid spacing used for the VR-CESM 0.25° mesh. (b) A depiction of 995 the transition from the global 1° resolution mesh through two layers of refinement to 0.25° . 996 (c) Topography height over the study area.	48
997 Fig. 2.	Mean precipitation and associated indices from VR-CESM and reference datasets over the 998 historical period, 1980-2005. Areas with statistically significance differences are marked 999 with stippling.	49
1000 Fig. 3.	Mean precipitation and associated indices from VR-CESM and reference datasets over the 1001 historical period, 1980-2005 (continued).	50
1002 Fig. 4.	Mean precipitation and associated indices from VR-CESM and reference datasets over the 1003 historical period, 1980-2005 (continued).	51
1004 Fig. 5.	2m average temperature (Tavg), 2m relative humidity (RH) and mean precipitation (Pr) av- 1005 eraged over the historical time period, along with average differences mid-hist and end-hist. 1006 Areas with statistically significance differences are marked with stippling.	52
1007 Fig. 6.	Differences of precipitation indices Pr (mm/day), SDII and R*mm between hist, mid and 1008 end average. Areas with statistically significance differences are marked with stippling.	53
1009 Fig. 7.	Differences of precipitation indices Pr (mm/year) and P*mm between hist, mid and end 1010 average. Areas with statistically significance differences are marked with stippling. Areas 1011 with no data are indicated in gray.	54
1012 Fig. 8.	Differences in specific humidity and horizontal wind patterns at 850hPa for moisture flux, 1013 and pointwise IVT (averaged over days with (a) $10\text{mm} < \text{Pr} \leq 40\text{mm}$ and (b) $\text{Pr} > 40\text{mm}$) 1014 for the cool season (October to March) averaged over 26 years. The minimum wind vector 1015 length is set to 0.5 m/s for better visualization. (Lower plot) Specific humidity and wind 1016 patterns are averaged over all days over <u>the cool seasons</u>	55
1017 Fig. 9.	Frequency distribution of <u>rainy</u> days (with $\text{Pr} \geq 0.1\text{mm/day}$) over the three time periods 1018 from all simulations dataset in four regions (with logarithmic vertical scale). (Note: Region 1019 (a) to (d) cover Washington and Oregon; California (except northern part, i.e. latitude no 1020 larger than 38°); Nevada and Utah; Arizona and New Mexico, respectively.)	56
1021 Fig. 10.	<u>The 95th percentile (P95) of precipitation constructed from all days for the historical period,</u> 1022 <u>1980-2005 and the changes over each future time period.</u>	57
1023 Fig. 11.	Differences of precipitation indices Pr and R*mm between warm and cool phases of ENSO 1024 over each time period.	58
1025 Fig. 12.	Changes of IVT for simulations under different phases of ENSO of wet season (October to 1026 March) over rainy days averaged yearly, with seasonal mean wind patterns at 850hPa (unit: 1027 m/s) (Note: The minimum wind vector is set to be 0.5 m/s, therefore, the wind less than 0.5 1028 m/s is also plotted at the minimum length for better visualization.)	59



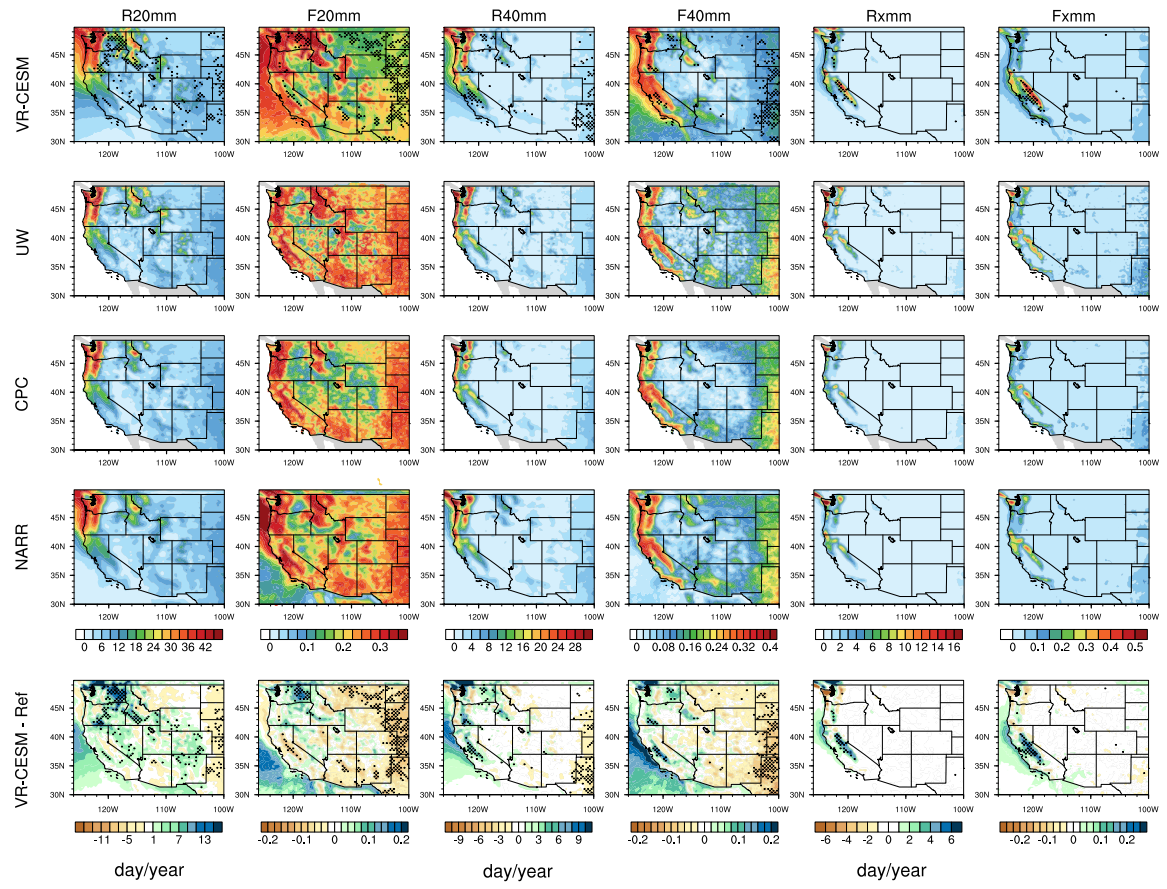
1029 FIG. 1. (a) The approximate grid spacing used for the VR-CESM 0.25° mesh. (b) A depiction of the transition
 1030 from the global 1° resolution mesh through two layers of refinement to 0.25° . (c) Topography height over the
 1031 study area.



1032 FIG. 2. Mean precipitation and associated indices from VR-CESM and reference datasets over the historical
 1033 period, 1980-2005. Areas with statistically significant differences are marked with stippling.



1034 FIG. 3. Mean precipitation and associated indices from VR-CESM and reference datasets over the historical
 1035 period, 1980-2005 (continued).



1036 FIG. 4. Mean precipitation and associated indices from VR-CESM and reference datasets over the historical
1037 period, 1980-2005 (continued).

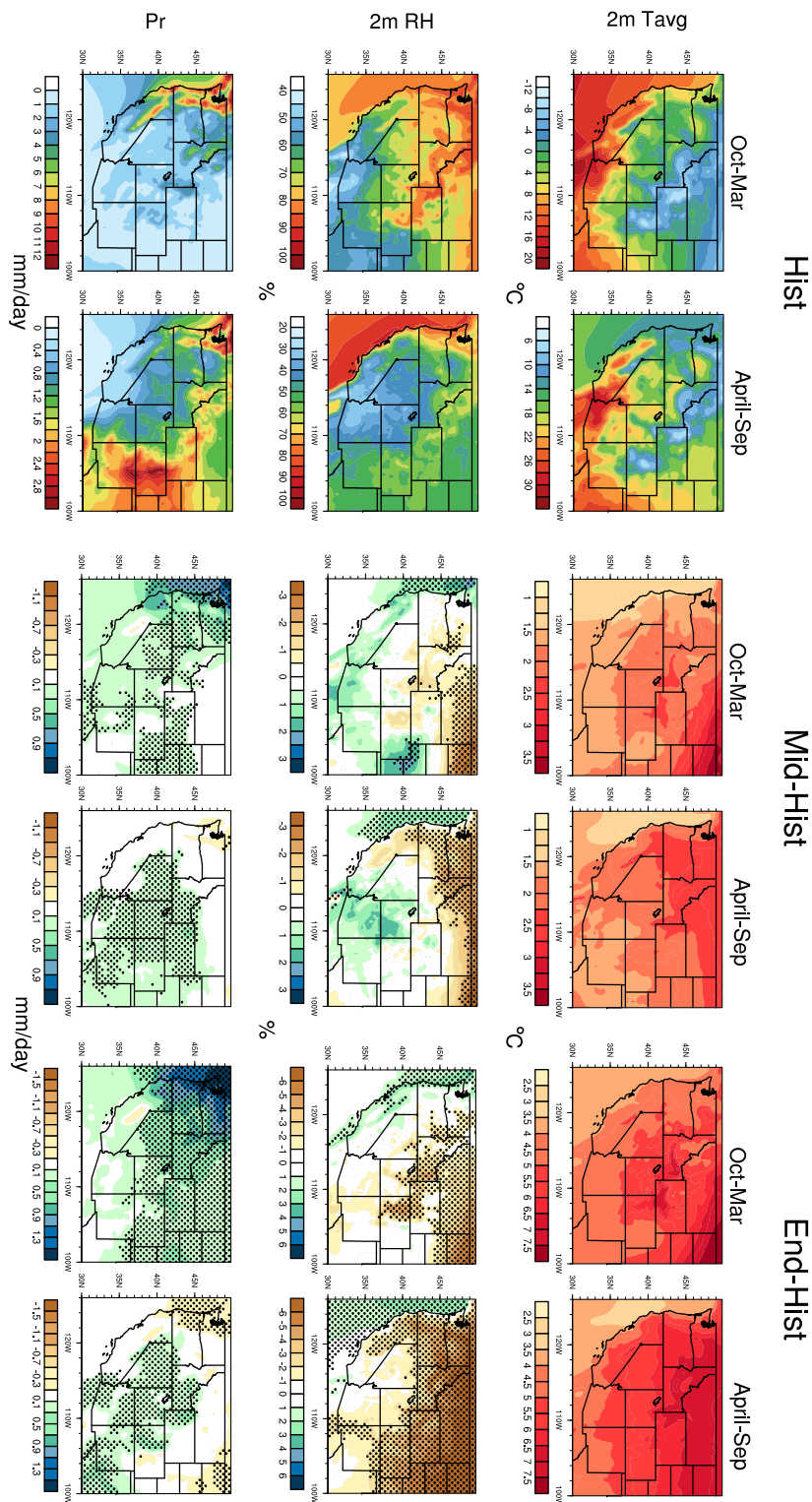
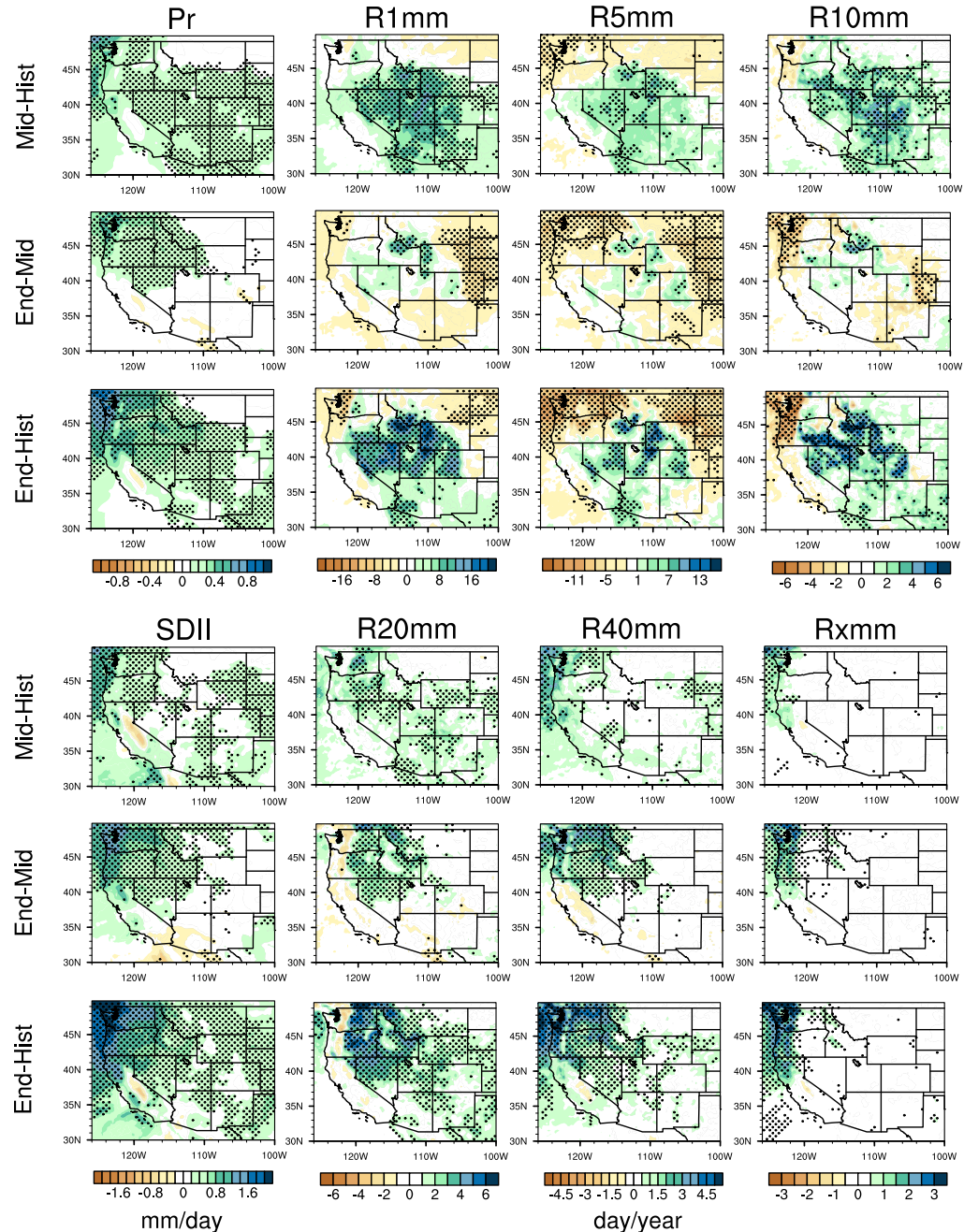


FIG. 5. 2m average temperature (Tavg), 2m relative humidity (RH) and mean precipitation (Pr) averaged over the historical time period, along with
1039 average differences mid-hist and end-hist. Areas with statistically significance differences are marked with stippling.



1040 FIG. 6. Differences of precipitation indices Pr (mm/day), SDII and R*mm between hist, mid and end average.
 1041 Areas with statistically significance differences are marked with stippling.

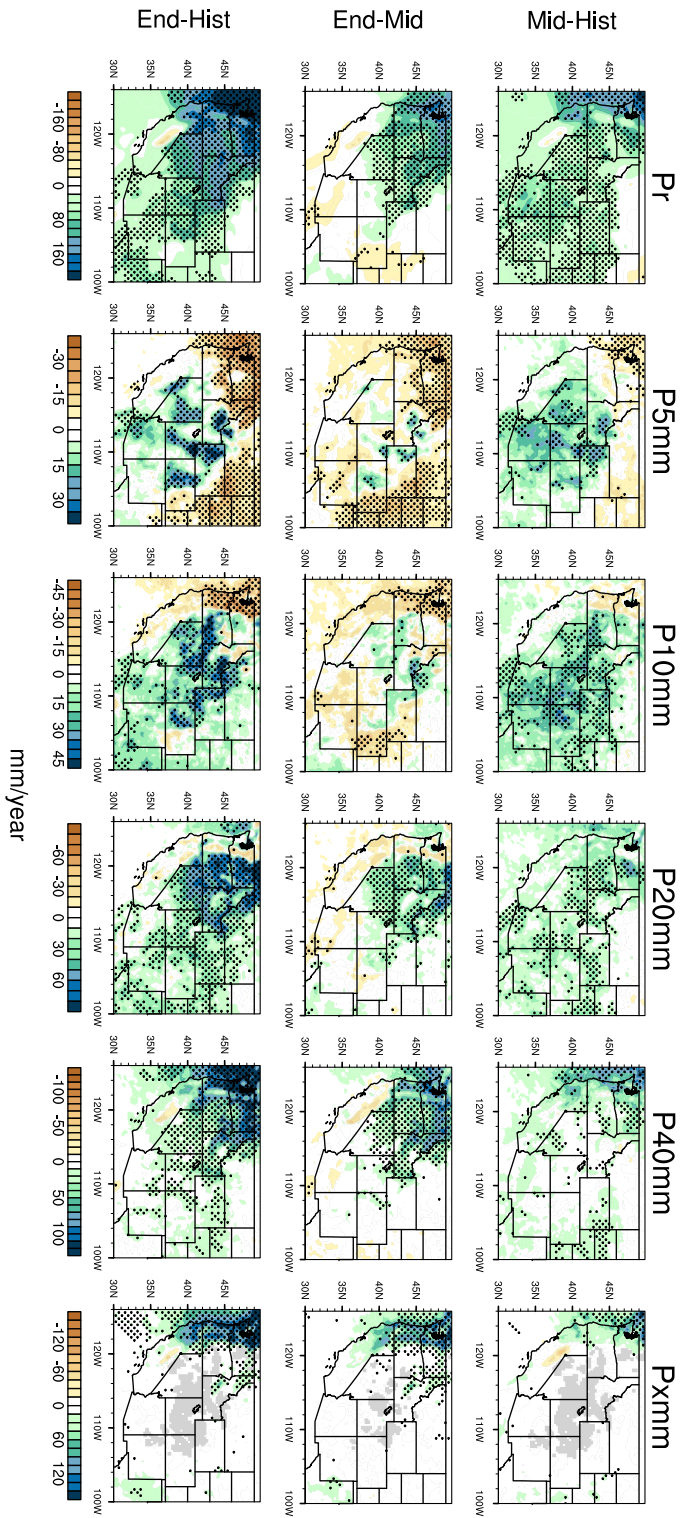
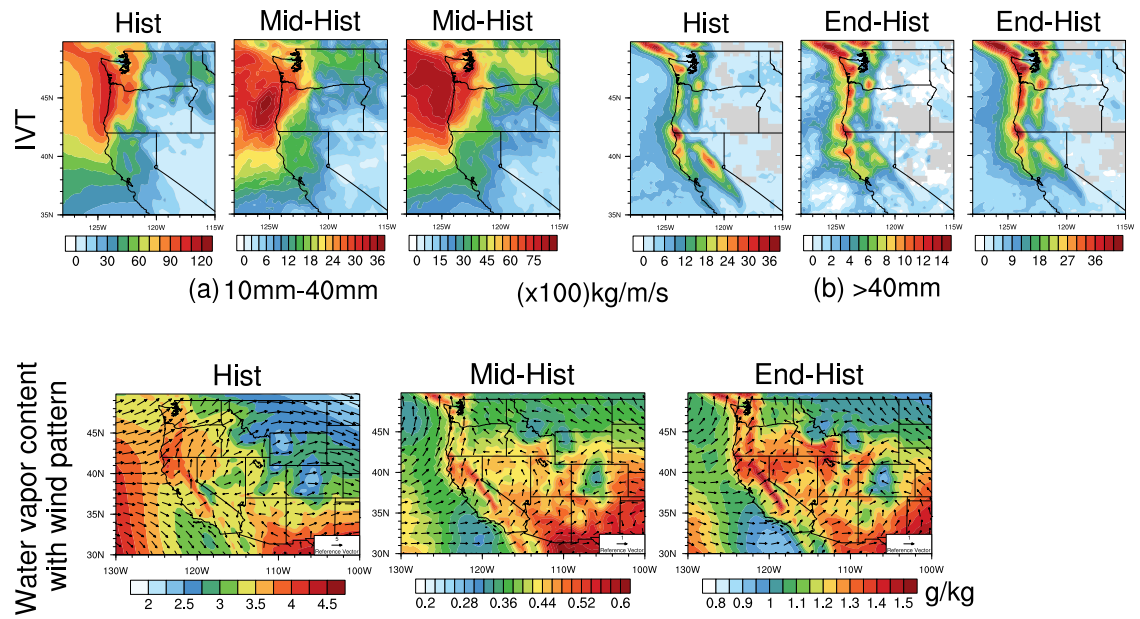


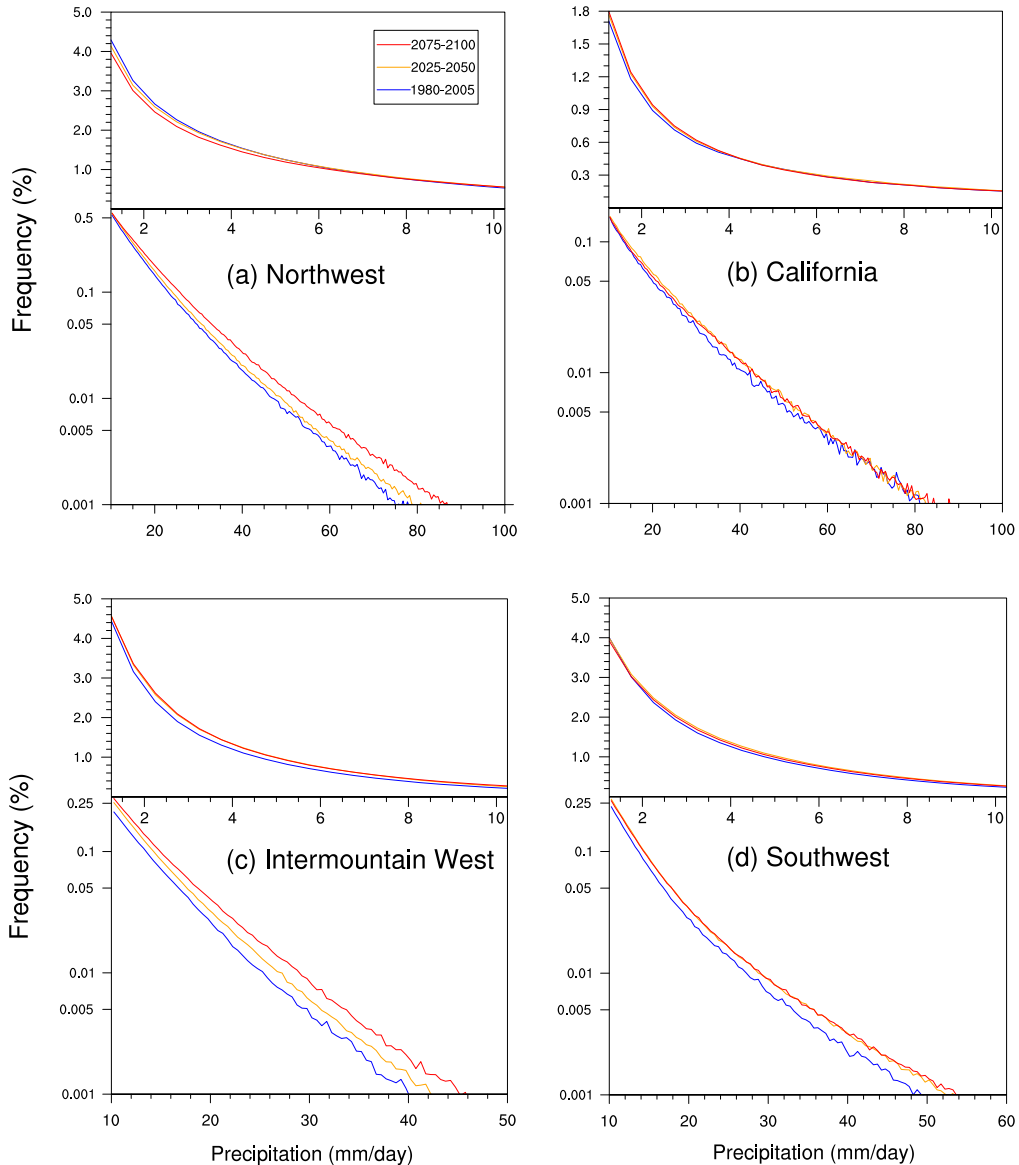
FIG. 7. Differences of precipitation indices Pr (mm/year) and P_{*mm} between hist, mid and end average. Areas with statistically significance differences are marked with stippling. Areas with no data are indicated in gray.

1042

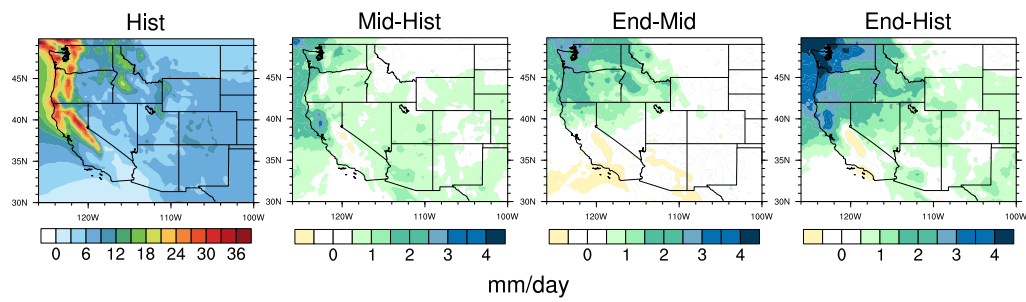
1043



1044 FIG. 8. Differences in specific humidity and horizontal wind patterns at 850hPa for moisture flux, and point-
 1045 wise IVT (averaged over days with (a) $10\text{mm} < \text{Pr} \leq 40\text{mm}$ and (b) $\text{Pr} > 40\text{mm}$) for the cool season (October
 1046 to March) averaged over 26 years. The minimum wind vector length is set to 0.5 m/s for better visualization.
 1047 (Lower plot) Specific humidity and wind patterns are averaged over the cool seasons.



1048 FIG. 9. Frequency distribution of **rainy** days (with $\text{Pr} \geq 0.1\text{mm/day}$) over the three time periods from all
 1049 simulations dataset in four regions (with logarithmic vertical scale). (Note: Region (a) to (d) cover Washington
 1050 and Oregon; California (except northern part, i.e. latitude no larger than 38°); Nevada and Utah; Arizona and
 1051 New Mexico, respectively.)



1052 FIG. 10. The 95th percentile (P95) of precipitation constructed from all days for the historical period,
 1053 1980-2005 and the changes over each future time period.

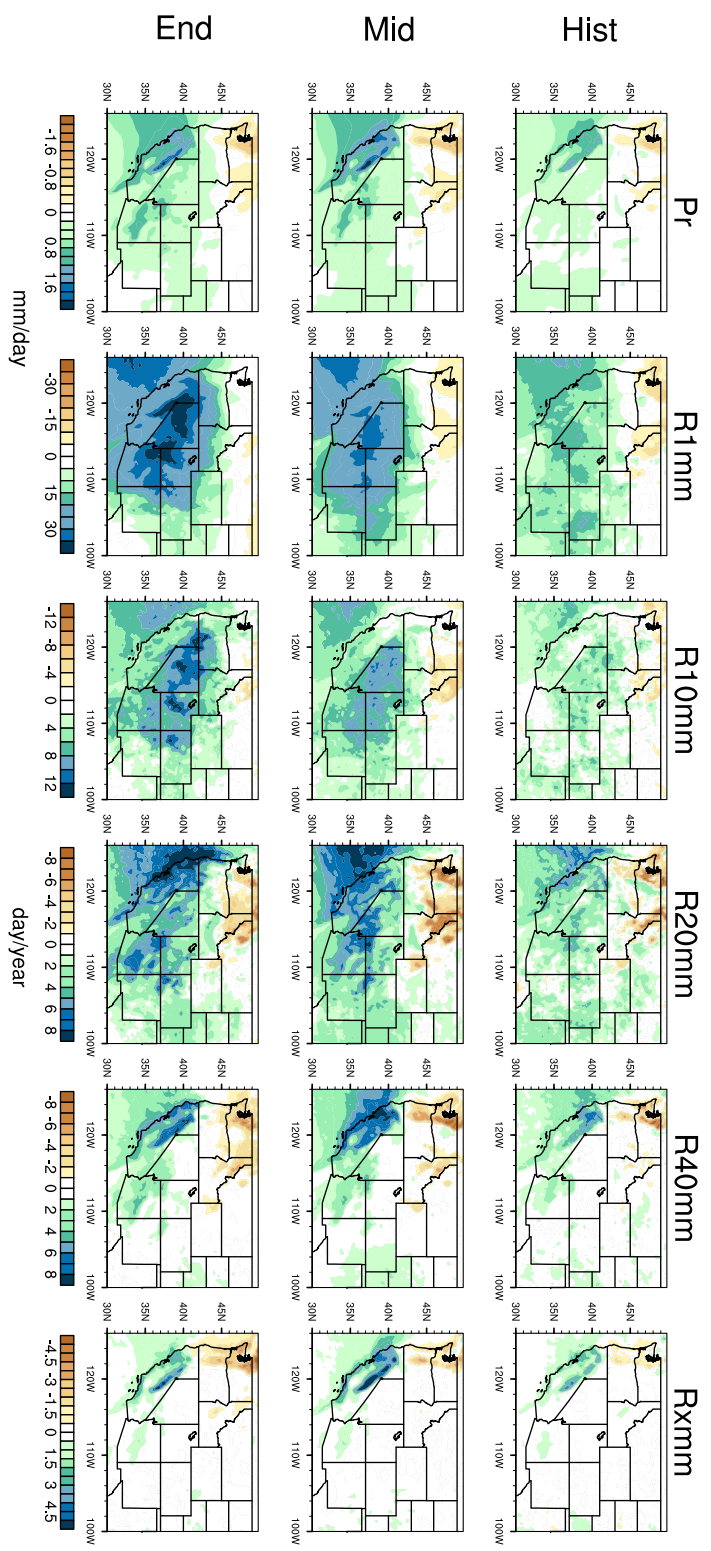
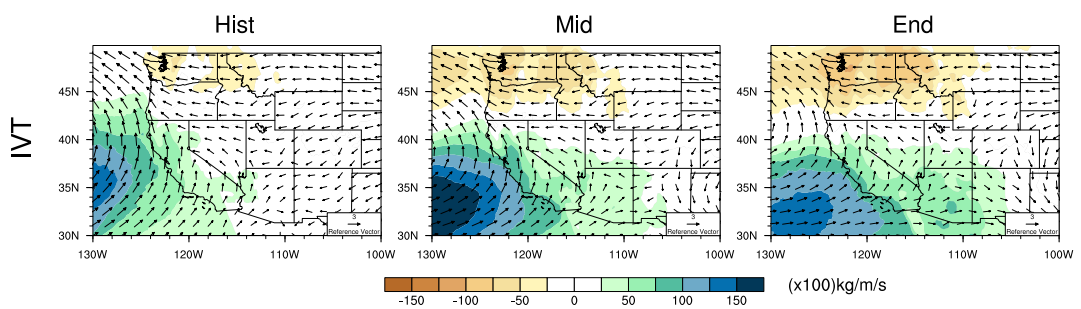


FIG. 11. Differences of precipitation indices Pr and $R_{\ast}mm$ between warm and cool phases of ENSO over each time period.



1054 FIG. 12. Changes of IVT for simulations under different phases of ENSO of wet season (October to March)
 1055 over rainy days averaged yearly, with seasonal mean wind patterns at 850hPa (unit: m/s) (Note: The minimum
 1056 wind vector is set to be 0.5 m/s, therefore, the wind less than 0.5 m/s is also plotted at the minimum length for
 1057 better visualization.)